UTILIZATION OF WASTE HEAT FROM HYDROGEN PRODUCTION

A case study on the Botnia Link H_2 Project in Luleå, Sweden

FREDRIK JONSSON

ANDREA MILJANOVIC

School of Business, Society and Engineering
Course: Degree Project in Energy Engineering
Course code: ERA403
Credits: 30
Program: M.Sc. in Energy Systems

Supervisor: Valentina Zaccaria
Examiner: Hailong Li
Costumer: Johan Granström, ABB
Date: 2022-06-08
Email:
fjn16007@student.mdu.se
amc17005@student.mdu.se

ABSTRACT

The global hydrogen demand is steadily increasing, and one way of accelerating the green hydrogen supply is to stimulate the green hydrogen economy. Utilization of waste heat from hydrogen production can increase the profitability of produced green hydrogen. Therefore, the aim of this study is to propose a system for integration of waste heat on the district heating (DH) network in Luleå, Sweden. Furthermore, an economic evaluation of the proposed system was conducted. In this study, the system was developed and investigated for two cases i.e. for a PEM and alkaline electrolyzer with an installed capacity of 100 MW. A large-scale heat pump and a heat exchanger were further added to the system to integrate the waste heat on the DH-network, while simultaneously providing cooling to the electrolyzer stack. The system was modelled for static conditions in the software MATLAB, with retrieved hourly DH data from Luleå Energi. The results showed that 203 060 MWh_{th} can be extracted from the PEM electrolyzer with a waste heat temperature of 79 ^{o}C, while 171 770 MWh_{th} can be integrated on the DH network annually. For the alkaline electrolyzer, 310 630 MWh_{th} can be extracted at a waste heat temperature of 80 ^{o}C, while 226 220 MWh_{th} can be integrated on the DH annually. The overall system efficiency is 94.7 % and 88.4 % for PEM and alkaline connected systems, respectively. Furthermore, the Levelized Cost of Heat (LCOH) is 0.218 SEK/kWh_{th} and 0.23 SEK/kWh_{th} for a PEM and alkaline connected system, respectively. For future scenarios with fourth generation of DH-networks, it is predicted that the LCOH can reach 0.018 SEK/kW_{th} for a PEM electrolyzer system, and 0.017 SEK/kW_{th} for an alkaline electrolyzer system. One conclusion that can be drawn from this study is that the utilized heat from the proposed system is price competitive in comparison with other thermal energy sources.

Keywords: PEM electrolyzer, alkaline electrolyzer, waste heat, district heating, LCOH

PREFACE

This study was conducted as a final project in fulfilment with the requirements for a degree in Master of Science in Energy Systems, at Mälardalen University in Sweden. The study was carried out in cooperation with ABB Sweden and Luleå Energi for the Botnia Link H_2 project, during the spring semester 2022.

We want to express our sincere and immense gratitude towards our supervisor Dr. Valentina Zaccaria; the outcome of this work would not be the same without your guidance and continuous support throughout the semester. Furthermore, we want to thank our examiner Prof. Hailong Li for insightful feedback on our work. Henrik Gåverud, Fredrik Udén and Thomas Öhlund at Luleå Energi for providing district heating data and for setting an initial direction for this study. Johan Granström at ABB for believing in us and allowing us to contribute to a fascinating and meaningful project. Last, but not least, thank you to Ola Norén at ABB who made this possible in the first place – and to all other people that have in some way made an impact on our work.

Västerås, June 2022

Fredrik Jonsson & Andrea Miljanovic

SUMMARY

Green hydrogen is a clean energy carrier that can help to decarbonize sectors with high CO_2 emissions, and thus contribute to the reduction of global greenhouse gas (GHG) emissions. One current drawback with green hydrogen is however the high pricing, in comparison to hydrogen produced by fossil fuels. Although, green hydrogen is produced in an electrolysis process which simultaneously provides by-products as heat and oxygen – and utilization of these by-products could potentially decrease production costs of green hydrogen. In this study, it is therefore of interest to determine how waste heat from an electrolysis process can be integrated into the DH-network in Luleå, and to evaluate the economic benefits of such an investment. More specifically, the aim is to investigate a heat recovery system for two electrolyzer types i.e. PEM and alkaline with an installed capacity of 100 MW. The proposed system consists of a heat pump unit that is used to upgrade the heat during periods of high DH supply temperatures, and a heat exchanger unit that transfers the heat when the DH supply temperatures are lower than the waste heat temperature.

A literature review was conducted to gain knowledge of state-of-the-art modelling approaches for the PEM electrolyzer, alkaline electrolyzer, and heat pump units. The system and its components were modelled for static conditions in the software MATLAB. Hourly DH-data for Luleå was retrieved from Luleå Energi and implemented in the model. Furthermore, the model was validated against the results of other studies, inter alia, Tiktak (2019) and Hu et al. (2017) to verify the accuracy of the proposed system.

For a PEM connected electrolyzer, the results showed that 203 060 MWh_{th} can be extracted from stack, while 171 770 MWh_{th} can be integrated on the DH-network in Luleå annually. The heat pump operates during 52 % of the year, and the heat exchanger is utilized during 48 %. The overall system efficiency is 94.7 %. The waste heat temperature is 79 ^{o}C and the calculated LCOH is 0.218 SEK/kWh_{th}, with electricity costs included. The results for an alkaline connected electrolyzer show that 310 630 MWh_{th} can be extracted from the stack at a waste heat temperature of 80 ^{o}C, while 226 220 MWh_{th} can be integrated on the DH annually. For this system, the heat pump is utilized during 48.5 % of the year while the heat exchanger operates during 51.5 %. The overall system efficiency is 88.4 % and the LCOH is calculated to be 0.23 SEK/kWh_{th}. For future scenarios with fourth generation of DH-networks, it is predicted that the LCOH can reach 0.018 SEK/kW_{th} for a PEM electrolyzer system, and 0.017 SEK/kW_{th} for an alkaline electrolyzer system. The future scenario however assumes that a heat pump is excluded, which reduces the investment costs by approximately 88 %.

The conclusions that can be drawn from this study is that the proposed system is able to utilize the waste heat from the electrolyzers for a competitive price, while providing essential cooling to the electrolyzer stack. Future scenarios also predict that the LCOH can be further decreased.

CONTENT

LIST OF FIGURES

LIST OF TABLES

NOMENCLATURE

Symbol	Description	Unit
[A]	[Area]	[m^2]
[Cp]	[Specific heat capacity]	[J/kg, K]
[F]	[Faraday constant]	[C/mol]
[H]	[Enthalpy]	[kJ/kg]
[h]	[Heat transfer coefficient]	[W/m^2, K]
[I]	[Current]	[A]
[i]	[Current density]	[A/cm^2]
[k]	[Thermal conductivity]	[W/m, K]
[L]	[Length]	[m]
[$\dot{m}$]	[Mass flow]	[kg/s]
[η]	[Efficiency]	[%]
[Nc]	[Number of cells]	[-]
[P]	[Power]	[W]
[p]	[Partial pressure]	[bar]
[Q]	[Heat transfer]	[W]
[R]	[Gas constant]	[J/mol, K]
[Rt]	[Thermal resistance of alkaline electrolyzer]	[°C/W]
[S]	[Entropy]	[kJ/K]
[T]	[Temperature]	[K]
[V]	[Voltage]	[V]
[Vo]	[Volume]	[m^3]
[W]	[Work]	[W]
[z]	[Number of free electrons]	[-]
[ε]	[Emittance factor of a material]	[-]
[λ]	[Membrane water content]	[-]
[υ]	[Kinematic viscosity	[m^2/s]
[σ]	[Conductivity of the material inside the PEM electrolyzer]	[-]

TABLE OF SUBSCRIPTS

Abbreviation	Description
act	Activation energy
amb	Ambient
an	Anode side of the electrolyzer
c	Convection
ca	Cathode side of the electrolyzer
ci	Temperature of cooling fluid that enters the electrolyzer
co	Temperature of cooling fluid that exits the electrolyzer
cond	Condenser
cool	Cooling fluid
DH	District heating
elec	Electrical
evap	Evaporator
gen	Generation
is	Isentropic
loss	Losses, such as heat loss.
mech	Mechanical
r	Radiation
ref	Reference (used in context such as reference temperature)
return	Return temperature of district heating network
rev	Reversible voltage of electrolyzer
s	Stack
sat, liq	Saturated liquid
sat, vap	Saturated vapour
supply	Supply temperature of district heating network
th	Thermal
tn	thermoneutral
WW	Waste water

ABBREVIATIONS

Abbreviation	Description
CHP	Combined heat and power
COP	Coefficient of performance
DC	Direct current
DH	District heating
GHG	Greenhouse gas
GWP	Global Warming Potential
HEX	Heat exchanger
LCOH	Levelized cost of heat
MEA	Membrane Electrode Assembly
ODP	Ozone Depletion Potential
PEM	Polymer Electrolyte Membrane
SOE	Solid Oxide Electrolyzer

DEFINITIONS

Definition	Description
Reference study	Study which is used to compare results with
Upgrading unit	Unit that increases the temperature of the waste heat
Waste heat	Losses in form of heat from the electrolyzer stack

1. INTRODUCTION

A total of 196 international parties signed the Paris Agreement in 2015 with the aim to limit global warming. The parties recognized that the global average temperature increase must be limited to 1.5 ^{o}C, to prevent dangerous environmental impact caused by climate change. In order to meet this goal, greenhouse gas emissions (GHG) must be reduced. The use of fossil fuels must therefore be substituted with renewable alternatives at a rapid pace (IRENA, 2020). The Swedish government has therefore formed a national framework for Sweden's climate goals, which is to achieve net zero GHG emissions by 2045. Domestic emissions should be reduced by 85 percent in comparison with the emission levels in 1990 to meet this goal (Government, 2021).

Green hydrogen is a clean energy carrier that can help to reduce GHG emissions in the industry, transportation, and energy sectors. Green hydrogen is produced in an electrolysis process powered by renewable electricity. The process does not emit GHG emissions, instead heat and oxygen are the resulting by-products (Dong et al., 2022). In consensus to the benefits of green hydrogen, the Swedish government identified the energy carrier as a key element to achieve the national climate goals. Therefore, a national hydrogen strategy was presented by the Swedish Energy Agency in November 2021. The strategy presents a pathway towards implementation of a hydrogen-based energy system and stimulation of a hydrogen economy (Setterwalls, 2021). The aim of the national hydrogen strategy is to have a 10 GW electrolyzer capacity installed by 2045. Potentially, this could reduce Swedish GHG emissions by 15-30 percent (Eriksson & Hallonsten, 2021).

The idea of using hydrogen in an energy system is not new, but it has received more interest in the last couple of years due to its potential to decarbonize sectors with high CO_2 emissions. The involvement to achieve a beneficial hydrogen economy has therefore increased among stakeholders (Ball & Wietschel, 2009). Production and storage of hydrogen, as well as utilization of the excess products, can unburden the energy system. Hydrogen offers flexibility and security in the system by providing electricity to the grid when there is a mismatch in production and demand, and the excess heat can also be utilized in a district heating network for a similar purpose (Dong et al., 2022).

Due to the increased interest in fossil free hydrogen, more studies on the production of hydrogen by electrolysis have been proposed in the last couple of years. To this day there is however a lack of studies on the topic of utilization of waste heat from hydrogen production by electrolysis. It is beneficial to investigate waste heat recovery as it can improve the system efficiency and lower the operational costs of hydrogen production, hence strengthen the green hydrogen economy. Tiktak (2019) has studied the amount of excess heat that can be utilized from hydrogen production, i.e., from the electrolysis process. Tiktak also suggests utilization alternatives for waste heat recovery and one of them is to implement the waste heat into a district heating network. Although, the author does not consider a solution for implementation on the network. This study therefore aims to investigate how the waste heat from electrolysis can be integrated on a district heating network.

1.1. Background

1.1.1. Hydrogen demand and types

The global demand for hydrogen is steadily increasing. According to IEA (2019) it has risen from 18.2 Mt to 90 Mt from year 1975 and 2020 respectively. Approximately 80 percent of the total hydrogen production was classified as brown or grey hydrogen in 2022. These types of hydrogen are produced by fossil fuels, which contributed to the release of 900 Mt CO_2 emissions in 2020 (Shiva Kumar & Himabindu, 2019; IEA, 2021). The demand for hydrogen is mainly dominated by the industry sector, where methanol and steel production are two processes that require a high hydrogen usage. In the future, a high potential use of hydrogen lies within the transportation and energy sector. Hydrogen-fuelled vehicles, aircrafts and marine vessels provide a good opportunity for decarbonisation of the transportation sector. For the energy sector, hydrogen storage can provide stability and flexibility for the energy system. With an overall increasing demand of hydrogen and solutions to support the energy transformation, governmental supported incentives and investments for hydrogen technologies are also increasing (IEA, 2019).

However, one drawback with green hydrogen is the high production cost in comparison to brown and grey hydrogen. The production cost of green hydrogen is 10-13 dollars per kilogram of produced hydrogen. Meanwhile, the production cost of brown and grey hydrogen is 2-3 dollars and 2-6 dollars respectively, per kilogram of produced hydrogen (SGH2, n.d.) As it can be interpreted, fossil free hydrogen is not yet economically beneficial to this day. However, the aim is to reduce the fossil free hydrogen production cost to 1 dollar per kilogram in one decade - and electrolysis is the leading production pathway towards accomplishing this goal (EERE, 2017).

1.1.2. Production of green hydrogen

Green hydrogen is produced by a process called electrolysis, which occur in an electrolyzer unit. The electrolyzer must be powered by electricity from renewable energy sources for the green hydrogen to qualify as a clean energy carrier (Brunel, 2021). This process only emits oxygen and heat into the atmosphere, therefore green hydrogen is referred to as a clean source of energy (Shiva Kumar & Himabindu, 2019).

Electrolysis occurs when water is split into hydrogen and oxygen through chemical reactions, which is driven by an electrical current. Both endothermal and exothermal reactions occur within the electrolyzer, where excess heat is produced from the latter reaction (Godula-Jopek, 2015). When an electric current is passed between two electrodes, water molecules will decompose into hydrogen and oxygen in the following generalized reaction (Ruuskanen et al., 2017):

$$H_2O_l \rightarrow H_{2(g)} + \frac{1}{2}O_{2(g)}$$

There are three types of electrolyzer technologies available today, these are Alkaline, Polymer Electrolyte Membrane (PEM) and Solid Oxide Electrolyzer (SOE) (Ruuskanen et al., 2017). However, Alkaline and PEM are the two currently commercialized technologies (Carmo et al., 2013). The main structure of the different electrolyzers are similar – it consists of an operational cell with a negative and positive electrode, called anode and cathode respectively. The anode and cathode are separated by an electrolyte which conduct ions. Bi-polar plates connects the cells in series which together form a stack, and the stack is further equipped with crucial components to keep the operational conditions of the electrolyzer at an optimal state. These parameters include temperature, concentration of electrolyte, flow of water, input power and nominal pressures (Olivier et al., 2017).

1.1.3. Proton exchange membrane (PEM) electrolyzer

The PEM electrolyzer is compact, and the electrolyte consists of a membrane which is surrounded by an anode and cathode. The anode is situated at the inlet of the cell, where water molecules decompose into ions and oxygen. After the decomposition, oxygen and part of the inlet water leaves the cell while the ions migrate through the membrane to the cathode side. This migration occurs under the presence of an electric field. At the cathode side, the ions are then reduced into hydrogen. The PEM cell structure and the half-reactions occurring in the cell are illustrated in Figure 1 (Naimi & Antar, 2018).

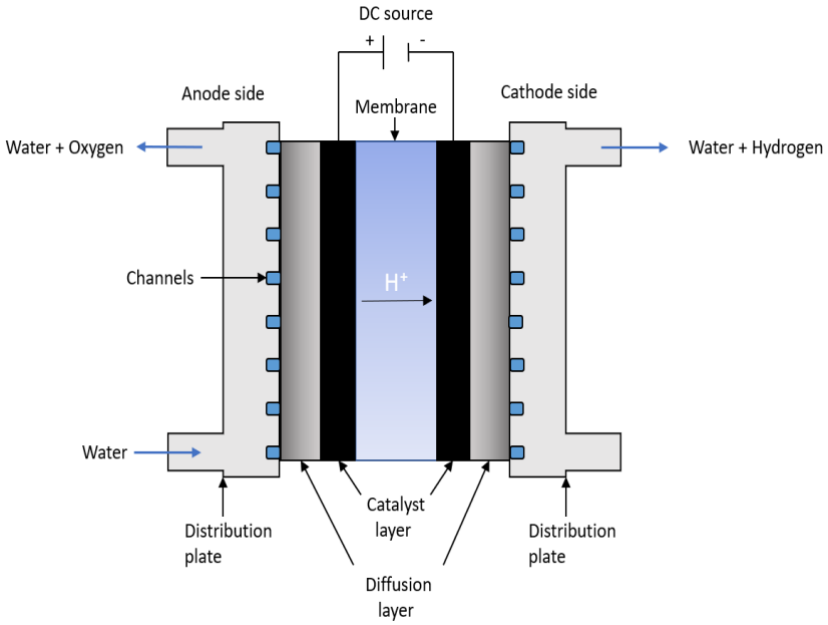

$$Anode: H_2O \rightarrow \frac{1}{2}O_2 + 2H^+ + 2e^-$$

$$Cathode: 2H^+ + 2e^- \rightarrow H_2$$

$$Overall: H_2O \rightarrow H_2 + \frac{1}{2}O_2$$

Figure 1. Schematics of a PEM electrolyzer inspired by Sood et al. (2020).

In the PEM electrolyzer, a porous catalyst layer is placed on each side of the membrane where the chemical reactions occur. The membrane and the catalyst layer together form what is called the Membrane Electrode Assembly (MEA). A current collector is placed around the MEA which connects the catalyst layer with the bipolar plate/distribution plate. Apart from providing the

ability to combine cells to form a stack, the bipolar plate is also present to provide structural integrity to the cell and channels for reactants and products (Falcão & Pinto, 2020).

The advantages of a PEM electrolyzer are that it allows for high current density (>2 A cm^2), high energy efficiency (70-80 %) (Carmo et al., 2013) and a fast response time whilst still producing very pure hydrogen (99.99 %). The cell voltage of the PEM electrolyzer typically works between 1.6 V to 2.0 V, while cell temperatures up to 90 ◦C are allowed to maximize the efficiency (Scheepers et al., 2021). However, modern PEM electrolyzers use noble metals such as IrO_2 and RuO_2 in the anode, and Pt and Pd in the cathode. The use of rare materials increase the price of PEM electrolyzers, which is why one of the challenges today is to reduce the production cost whilst still maintaining a high efficiency (Carmo et al., 2013).

1.1.4. Alkaline water electrolysis

The main difference between the alkaline and PEM technologies, is that the alkaline electrolyte consists of a liquid solution instead of a membrane. The liquid solution is surrounded by anode and cathode. A diaphragm separates the anode and cathode from each other for the purpose of keeping fluctuating product gases at one electrode (Carmo et al., 2013). The reactions occur under presence of an electric current, which is why a negative terminal from a direct current (DC) power unit is connected to the cathode. At the cathode, electrons are consumed by hydrogen ions to form hydrogen. In order to keep the electrical charge, hydroxide ions migrate through the separator from the cathode to the anode. The hydroxide ions release electrons - which returns to the positive terminal of the DC power. Finally, oxygen is released at the anode side and the produced hydrogen is collected at the cathode side (Zeng & Zhang, 2010). An illustration of the alkaline cell and the occurring chemical reactions can be seen in Figure 2.

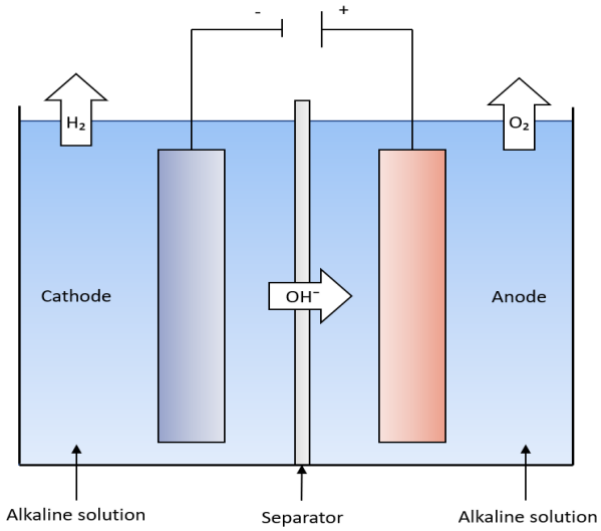

$$Anode: 2OH^- \rightarrow H_2O + \frac{1}{2}O_2 + 2e^-$$

$$Cathode: 2H_2O + 2e^- \rightarrow H_2 + 2OH^-$$

$$Overall: H_2O \rightarrow H_2 + \frac{1}{2}O_2$$

Figure 2. Schematics of an alkaline electrolyzer inspired by Bodner et al. (2015).

Potassium hydroxide is usually used as an electrolyte to avoid corrosion, while the electrode material typically consists of nickel due to low costs (Zeng & Zhang, 2010). The cell voltage is typically 1.8-2.4 V (Carmo et al., 2013), the operational temperature is ~30-80 ◦C and the efficiency is 60-80 % (Shiva Kumar & Himabindu, 2019).

The alkaline electrolyzer is considered as a mature technology, ready to scale up to the MW range. It is also cost effective in comparison to the PEM electrolyzer, which is considered as another advantage. Additionally, the used components for alkaline electrolyzers are rather durable which results in a longer technical lifetime of the unit (Carmo et al., 2013).

However, there are drawbacks for the alkaline electrolyzer technology, which include low partial load range, limited current density and low operating pressure. First, the separator does not completely prevent the gases from diffusing to the other side. This results in a loss of efficiency – since accidently cross-diffused oxygen will be catalysed back to water together with hydrogen that is present on the cathode side. Furthermore, mixing (when the hydrogen diffuses from the cathode side to the oxygen-rich anode side) is also present which decreases the safety and efficiency of the system. The mixing is particularly extensive at a low load level (<≈40 %), which drastically increases the explosion risk. This could be an issue when the alkaline electrolyzer is connected to intermittent electricity sources such as sun or wind. Due to high ohmic losses in the system, the second disadvantage with alkaline electrolyzers is the low achievable current density (0.1-0.4 A/cm^2). The third drawback is that the alkaline electrolyzer is unable to operate at high pressures, which leads to a bulky and large stack design (Carmo et al., 2013).

1.1.5. Botnia Link H2 Project

ABB Sweden, Uniper and the Port of Luleå are planning to build a hydrogen hub at Luleå harbour. This project is currently under a selection process for government incentives for national hydrogen strategies with the aim to connect and decarbonize the marine, industry, and energy sectors in Luleå (SVI, 2021). Production of green hydrogen will occur in a large-scale electrolyzer, with an installed capacity of 100 MW. The electrolyzer will be powered by electricity from the grid and on- and off-shore wind turbines. In order to maximize the system efficiency of the hub, further plans are to utilize all by-products from hydrogen production, such as heat and oxygen, and to refine the hydrogen into green methanol by synthesis. See Figure 3 for system schematic of the hub.

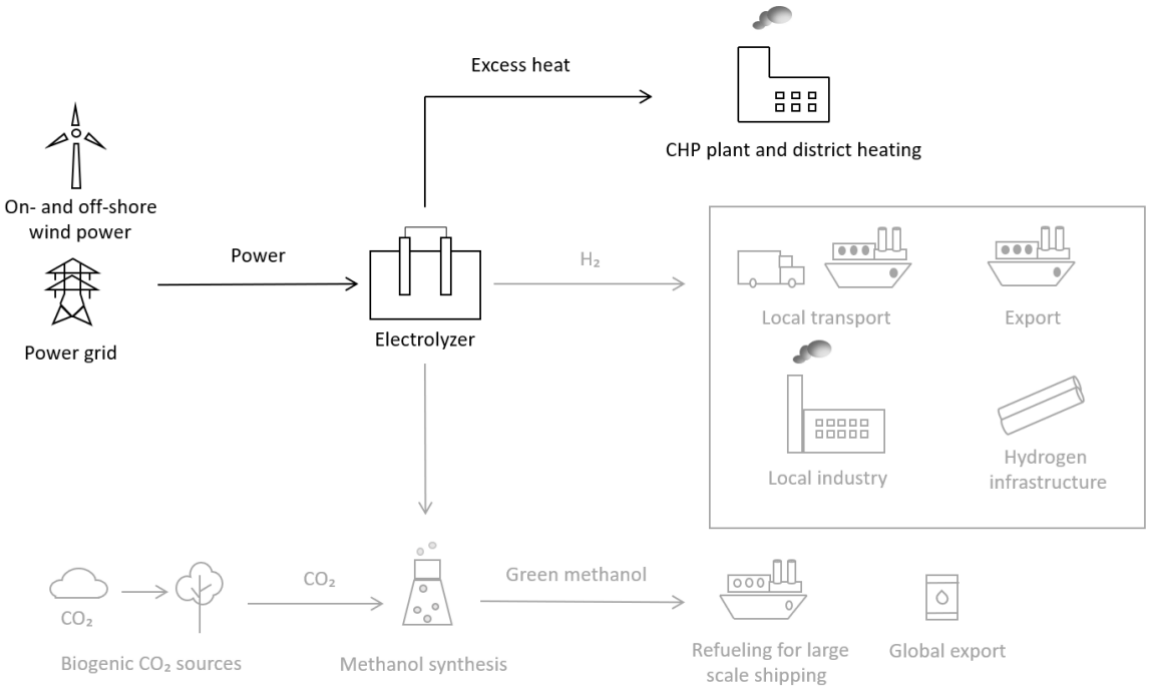

Figure 3. System schematic of the planned hydrogen hub in Luleå, Sweden.

The Botnia Link H2 project can be divided into two phases. In the first phase of the project, the aim is to implement the 100 MW electrolyzer for hydrogen supply to the local transportation and industry sector. Primarily, it is although of importance to develop a hydrogen infrastructure that enables a reliable supply of the produced hydrogen. In this phase, utilization of excess products from hydrogen production should also be investigated.

In the second phase of the project, the aim is to produce green methanol with the produced hydrogen. Green methanol can be used as a substitute for conventional fuel needed for large scale marine vessels, meaning that one of the targets of producing green methanol at Luleå harbour is to provide refuelling of incoming vessels. The other aim is to provide European and global export of green methanol. The biogenic CO_2 sources that are needed for the methanol synthesis is planned to be provided by local suppliers.

To this day, the Botnia Link H2 project is currently in the very early stage of development. The electrolyzer technology has not yet been chosen and technical solutions for utilization of waste products have not been investigated. Thus, the stack might consist of either Alkaline or PEM electrolyzers. The focus of this case study will therefore be directed towards utilization of waste heat from the electrolysis process. More specifically, the alternative that will be investigated is how the useful excess heat can be integrated into the district heating (DH) network in Luleå, owned by Luleå Energi. Utilization of waste heat can provide economic and environmental benefits and improve the system efficiency. Usually, the electrolyzer stack would need a cooling tower which comes with additional costs. However, in this study the cooling circuit will be integrated into the DH network to increase the revenue and overall system efficiency.

Luleå Energi is currently utilizing waste gases from a local steel industry (SSAB) in a combined heat and power (CHP) plant for a thermal baseload supply in the DH-network. The CHP-plant

is jointly owned by Luleå Energi and SSAB through a separate production company (LuleKraft). Luleå Energi is further aiming to have a completely fossil free heat generation in the future. Therefore, it is also of interest for Luleå Energi to investigate the suitability of waste heat from electrolysis. The DH-network in Luleå is classified as a third generation of district heating technology, which is also the most common in Scandinavia to this day according to Werner (2017). For third generation of DH networks, pressurized water is used as an energy carrier with supply temperatures often under 100 °C (Lund et al., 2014). In Sweden however, the supply temperature is correlated with the outdoor temperature. Lower outdoor temperatures require higher supply temperatures – which can be over 100 °C during winter periods (Werner, 2017). When integrating low-temperature waste heat into the third generation of DH-network, upgrading technologies are often required due to the high operating temperatures according to Sayegh et al. (2018).

1.1.6. Waste heat recovery units

There are different technologies that can be used for waste heat recovery. The main examples are recuperators, waste heat recovery boiler, regenerators, heat exchangers and heat pumps. The suitability of the mentioned alternatives is mostly dependent on the fluid type and temperature of the heat source, and the intended application. A waste heat recovery boiler is used to recover low to medium exhaust gases to steam, while recuperators are a variant of heat exchangers that are suitable for increasing the temperature of exhaust gases. These recovery units are thus not suitable for a DH-application. Instead, heat exchangers that transfer heat between two fluids, or a heat pump that can transfer heat from both air and liquid sources are more appropriate alternatives. A heat pump operates by transferring heat from a heat source to a heat sink with low electricity consumption (Jouhara et al., 2018).

For this case study, it is of interest to upgrade the waste heat to a specific DH supply temperature. Depending on the temperature of the waste heat, a heat exchanger could be a suitable alternative. However, a heat pump offers more flexibility in terms of the temperature upgradation interval – it can be dimensioned to upgrade heat for specific interval that might be needed for the DH-network in Luleå. While for a heat exchanger, the possible upgrading temperature interval is narrower. Assuming no leakages of refrigerants and fossil free supply of electricity, heat generation by a heat pump is also considered to be essentially carbon-free (Averfalk et al., 2017). A heat pump is therefore chosen as a primarily upgrading unit for this case study. The specific type of heat pump is further presented in chapter 3.3.

1.2. Purpose

The purpose of this study is to determine how waste heat from a PEM and alkaline electrolyzer can be utilized and integrated in the district heating network in Luleå, Sweden, to increase the system efficiency. It is also of importance to analyze the economic opportunities for utilization of the waste heat.

1.3. Research questions

- How much heat can be extracted from a PEM and alkaline electrolyzer stack with an installed capacity of 100 MW?
- How much waste heat can be utilized on the DH-network in Luleå?
- What is the performance of the overall system?
- What is the Levelized Cost of Heat of the utilized waste heat and what are the factors that affect the economic feasibility?

1.4. Delimitation

This study only investigates how the waste heat from large-scale PEM and alkaline electrolyzers can be utilized. Additionally, the cells in the electrolyzer stack are all considered to have the same performance. In reality, this is not the case since cells that are placed in the outer part of the stack experience different heat transfer in comparison with the core cells.

The model will be developed for static conditions, and pressure losses in pipes and pre-heating of incoming water into the electrolyzer stack will be neglected. Furthermore, only the extracted heat from the electrolyzer stack is investigated – excess heat from hydrogen compression is not considered in this study.

2. METHOD

The methodology chapter gives an overview of the taken approach for this case study, where the different stages during the development of this study is briefly described.

The methodology approach for the model development of this case study consisted of five stages: a literature study, data collection and management, model development, model validation and economic evaluation. Figure 4 shows the systematic approach that was followed throughout the study. Due to convenience, the literature study was carried out in parallel to developing the model since the model development itself consisted of several steps. These steps involved modelling of both PEM and alkaline electrolyzers, heat pump modelling and heat exchanger modelling. Therefore, an effective approach was to develop a literature framework for each modelling step before continuing to the next. Accordingly, each step of the model was validated against similar theoretical models from the literature. An economical evaluation of the generated heat from the proposed system was performed lastly.

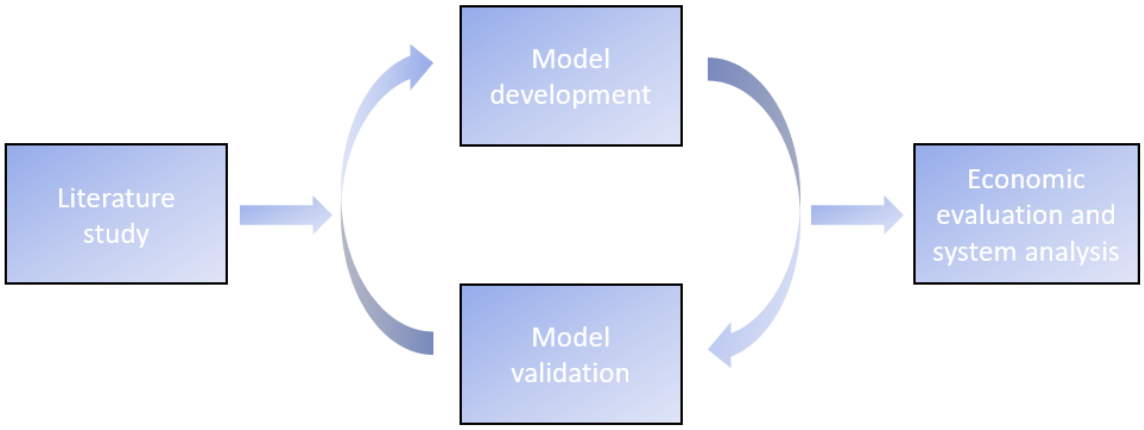

Figure 4. Methodology approach.

2.1. Literature study

A literature study was performed to gain more knowledge about fundamental electrolyzer technologies and the possibilities to integrate the waste heat into a DH-network. Information about state-of-the-art PEM, alkaline and heat pump modelling was investigated for model development, and thus to be able to suggest a feasible technical solution for waste heat integration on the DH-network in Luleå. Previous research on the mentioned topics was retrieved from the search engines Science Direct, Primo by Mälardalens University, and Google Scholar. The key search words used for this study was *modelling PEM electrolyzer, modelling alkaline electrolyzer*, *waste heat potential*, *upgrading waste heat* and *high temperature heat pump,* where peer-reviewed articles have been prioritized.

2.2. Data collection and management

Hourly raw operating data for a specific point in the DH-network in Luleå was received from Luleå Energi for year 2019 in Excel-format. The data consisted of information about total heat supply, outdoor temperature, demand- and return side temperatures and the volume flow in the DH-network. This information was essential for dimensioning the heat pump and heat exchanger. However, the received data is undisclosed for publicity which means that full transparency of truthful values is not possible to offer in this study. The hourly supply and return temperatures are therefore divided by the yearly mean temperature to illustrate deviations of the raw data in Figure 5 and 6 respectively. The processed data is illustrated in Figure 7 and 8. The supply and return side temperatures will compose an example for how all components of the data has been managed. The raw data diverges during certain periods of the year. Inaccuracy in data occurs as a result of operational shut-down due to maintenance or a loss of data.

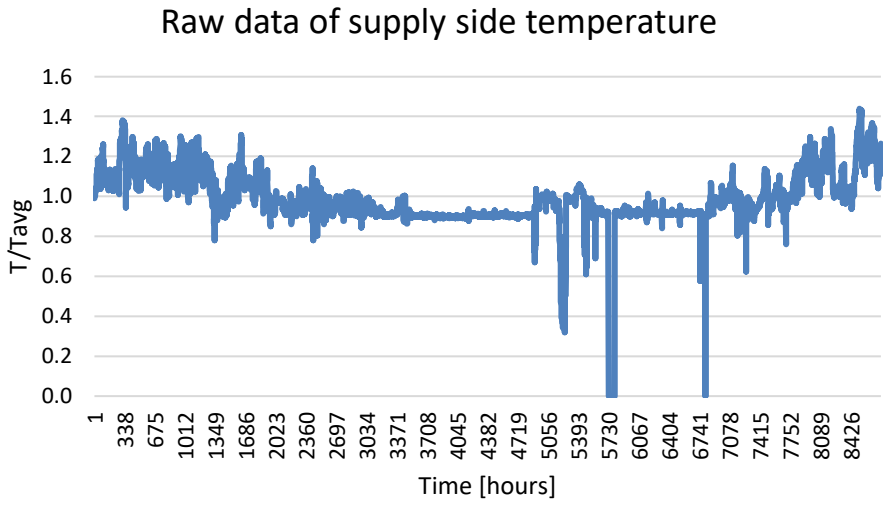

Figure 5. Raw data of the supply side temperature during 2019.

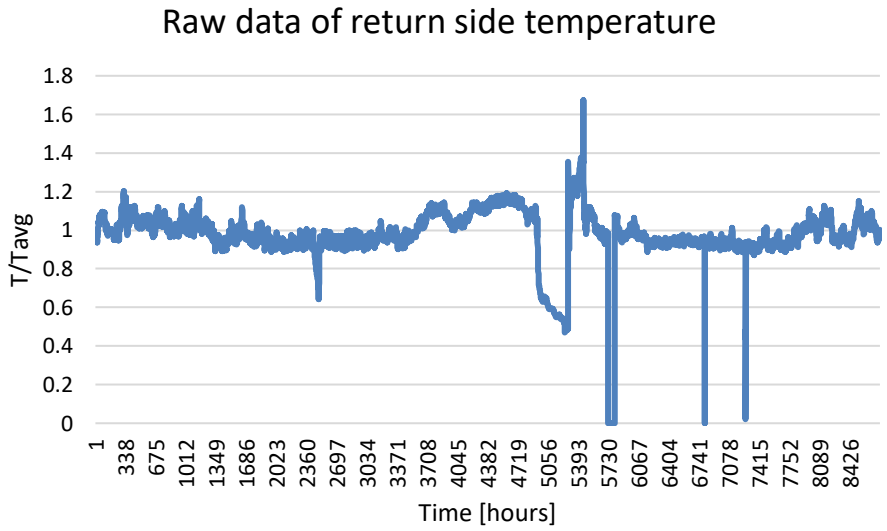

Figure 6. Raw data of the return side temperature during 2019.

During periods of inaccurate raw data, the supply and return temperatures was modified and assumed to be a function of the outdoor temperature. The final processed supply temperatures are represented in Figure 7 and 8. Deviations from an ideal operation are still present to some extent, however, they are not tampered with since the cause for these events are unknown. Although, the undisclosed data works within a temperature domain which is similar to the figures below, and thus decisive for the accuracy of the processed data.

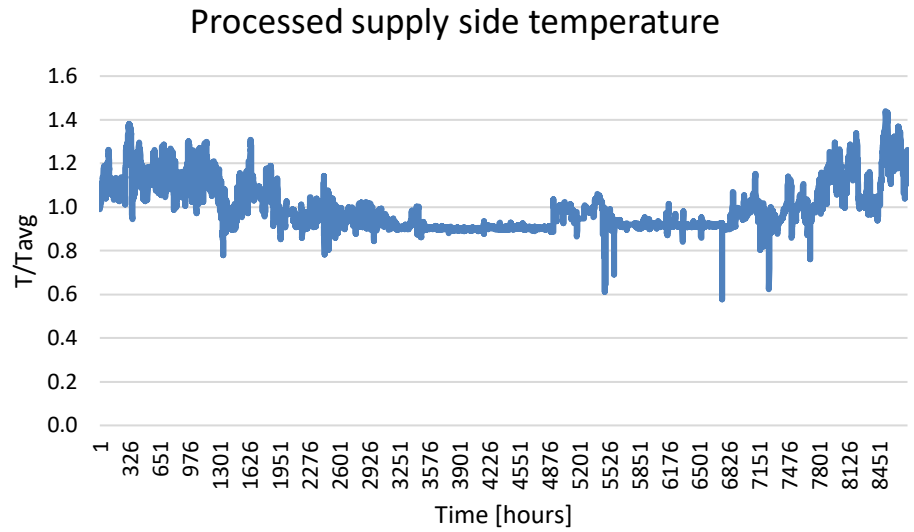

Figure 7. Graph of the processed supply side temperature.

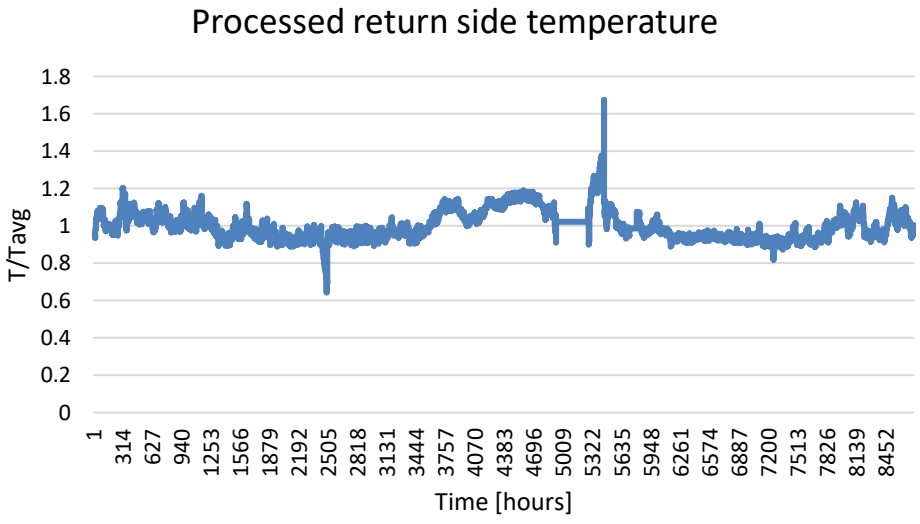

Figure 8. Graph of the processed return side temperature.

2.3. Model development and validation

The model of the proposed system was developed in the software MATLAB. MATLAB is a programming software that can be used to create models by letting the user write mathematical scripts and receive outputs as results (Mathworks, n.d.), which is the reason for the use of the software in this study. Additionally, CoolProp is used as a plugin program in MATLAB to calculate the properties of the refrigerant used in this study (CoolProp, n.d.). The model of this case study consists of two sub-models, an electrolyzer model and a system model. As mentioned in the opening of the method section, the model development is therefore divided into the following steps in this study:

Step 1: Modelling of PEM and alkaline electrolyzers. Both electrolyzer models consists of three parts; an electrochemical model, a thermal model and a cooling model. The electrochemical model aims to simulate the electrochemical properties of the electrolyzer, i.e. the electrical efficiency and cell voltage at 100 MW input power. The thermal model simulates the thermal losses in the electrolyzer stack and the amount of thermal energy that can be utilized as waste heat. The cooling model calculates the input and output temperatures of the cooling medium, and the mass flow required to keep the electrolyzer stack at suitable operating conditions.

Step 2: Modelling of the total system, which aims to simulate the total heat transfer from the electrolyzer stack to the DH-network. The values of the required mass flow and cooling temperatures are imported into the total system model, along with the data of DH temperatures received from Luleå Energi. Total energy output to the DH-network, required dimensions of the heat pump and heat exchanger, and the electricity consumption are received from this model.

Step 3: Economical calculations of the generated heat from the system. The heat output and electricity consumption are retrieved from the system model to analyze the price competitiveness. Additionally, a sensitivity analysis of the calculated cost is performed for parameters of uncertainty.

The modelling of the electrolyzer and heat pump was be performed by utilizing state-of-the-art models from retrieved literature. There is a lack of ready-to-use models that are developed for the purpose of integrating waste heat from electrolyzers into the DH-network. In this study, several models are therefore pieced together into a system model. The model of the proposed system is validated against the results from the study by, inter alia, Tiktak (2019) and Hu et al. (2017) to acknowledge the legitimacy of this study. It is not possible to validate the model through experiments; therefore, it is of importance that the equations used in the reference studies are verified experimentally. This allows the model to be indirectly experimentally validated.

2.4. Economic evaluation

The economic analysis for the generated heat and thus proposed system was conducted by evaluating the Levelized Cost of Heat (LCOH). LCOH is a measure of the average revenue per generated unit of heat that would be required for the investment to break even, during the lifetime of the system (EIA, 2022). It could also be interpreted that LCOH is the cost for producing one unit of energy. This evaluation is often used to compare different investment alternatives while it also gives a good indication of the profitability of a project for investors. LCOH is also a favourable method to use when the potential revenue is unknown which, in contrary, is an essential factor when calculating Life Cycle Costs (LCC) or Pay-Back time for an investment (Papapetrou & Kosmadakis, 2022).

For this case study specifically, it is of interest to determine the average cost of one kilowatt hour of generated heat from the heat pump and heat exchanger. Due to uncertainty of the future district heating pricing strategy and potential revenue, LCOH was chosen as a method for the economic evaluation. The LCOH was performed on Capital Expenditure (CAPEX) and Operational Expenditure (OPEX) costs, without considering possible reductions in costs by subsidies or incentives.

3. LITERATURE STUDY AND THEORETICAL BACKGROUND

In this chapter, modelling approaches for PEM and alkaline electrolyzers are described from retrieved literature. Furthermore, heat pumps and connection alternatives for the DH-network are presented.

3.1. Modelling PEM Electrolyzer

A modeling approach of a PEM electrolyzer have been suggested by several authors, among them are Tiktak (2019), Falcão and Pinto (2020), and Lebbal and Lecœuche (2009). In the studies by the mentioned authors, PEM electrolyzers have been modeled for different purposes. What is common in these studies, however, is that the authors propose that the PEM electrolyzer should be broken down into at least two parts: an electrochemical model and a thermal model. This is valid if it is of interest to model the temperature variance of the electrolyzer, which is also what Olivier et al. (2017) advise in their review of different PEM electrolyzer modeling approaches. The electrochemical model shows the relation between the cell voltage and current density, while the thermal model illustrates the produced heat from the electrolyzer. It is suggested that these parts should be modeled separately and later coupled into a final model.

In the study of Tiktak (2019), the aim is to determine the useful amount of excess heat that is produced by a PEM electrolyzer. Tiktak therefore suggests that a third part should be added to the model of the electrolyzer i.e., a cooling circuit model. The cooling medium in the circuit will circulate through the stack and extract the excess heat.

3.1.1. Electrochemical model

The purpose of the electrochemical model is to derive the relationship between the electrical current density and cell voltage at different operating conditions (Ruuskanen et al., 2017). There are several authors that have suggested a modelling approach for the electrochemical model, inter alia, Tiktak (2019), Awasthi et al. (2011) and Ruuskanen et al. They chose to model for a single cell due to convenience. The retrieved values are then multiplied with the total amount of cells in the stack to receive results for the electrolyzer as a whole. Falcão and Pinto (2020) have also performed a technical review of different modelling approaches. It is clear that most authors agree to use the same approach to calculate the cell voltage in the review of Falcão and Pinto, however different equations and parameters are used for the same purpose.

The minimum required energy to split the water into oxygen and hydrogen by means of electrical energy is called thermoneutral voltage. An operating cell at thermoneutral voltage does not consume or produce heat (Tiktak, 2019). The thermoneutral voltage (V_{th}) for one cell is approximated to be 1.481 V at standard conditions according to Falcão and Pinto. Tiktak also presents this value, and the author suggest that it can be used to validate the real cell voltage. This is because the real cell voltage should be higher than the thermoneutral voltage. The real cell voltage is higher since it must compensate for activation energy and ohmic losses of the cell, thus an overpotential is needed. The cell voltage is commonly represented open-circuit voltage (U_{ocv}), activation overpotential (U_{act}) and ohmic overpotential (U_{ohm}). The open-circuit

voltage, U_{ocv}, represents the cell potential between anode and cathode when the current is zero (Lebbal & Lecœuche, 2009).

$$V_{cell} = V_{ocv} + V_{act} + V_{ohm} \quad (1)$$

According to Falcão and Pinto, the open-circuit voltage (V_{ocv}) can be derived from the Nernst equation (eq. 2). This equation involves the universal gas constant (R), temperature (T), Faraday constant (F), partial pressures of reactants (p_x) and the reversible voltage (V_{rev}). The reversible voltage is the lowest voltage that is needed in order for water to decompose.

The partial pressures are calculated differently depending on the study. Ruuskanen et al. use a method which is based on Dalton's law. Fragiacomo and Genovese (2019) however suggests that the partial pressures can be calculated by an expression of the ideal gas law and the molar concentration of each product. Oxygen is only present at the anode, where water is oxidized, which means that the partial pressure of the product is calculated for at the anode. As for the partial pressure of hydrogen, it is calculated for at the cathode where the water is reduced. However, the flow of water is present throughout the anode, membrane and cathode which means that the partial pressure of water is calculated for all three stages. Oftentimes, the partial pressure of water is however assumed to be 1.

$$V_{ocv} = V_{rev} + \frac{RT}{2F}\left[\ln\left(\frac{p_{H_2}\sqrt{p_{O_2}}}{P_{H_2O}}\right)\right] \quad (2)$$

Activation overpotential is needed to activate electrochemical reactions at the anode and cathode. The authors Marangio et al. (2009), Awasthi et al. (2011) and Tiktak (2019) suggests that the activation overpotential should be calculated by using the Butler-Volumer equation, where the exchange currents (i_o) and charge transfer coefficients (α) at the anode and cathode are taken into consideration. The exchange current density holds a significant effect on the activation overpotential. The exchange current densities at both the anode and the cathode are dependent on the operational temperature of the stack (Abdin et al., 2015). In the study of Awasthi et al. the value of the charge transfer coefficients was iterated for to be fitted into their model, while Marangio et al. assumed a value of 2 and 0.5 at the cathode and anode, respectively. Tiktak however assumed a value of 0.5 for the cathode and anode, and suggested that the activation overpotential can be calculated according to Equation 3.

$$V_{act} = \frac{RT_a}{\alpha_a zF}\ln\left(\frac{i}{i_{0,a}}\right) + \frac{RT_c}{\alpha_c zF}\ln\left(\frac{i}{i_{0,c}}\right) \quad (3)$$

The ohmic overpotential occurs due to the losses in the materials inside the cell and it can be divided into electronic and ionic resistance (Ruuskanen et al., 2017). Electronic resistance is caused by the flow of electrons through the electrode material, while the ionic resistance is caused by the flow of ions through the membrane (Koroglu et al., 2019). The ionic resistance does however create a higher loss than the electronic resistance. The ohmic overpotential is

influenced by the current density (i_{cell}) thickness of the cell material (δ) and material conductivity (σ). The material conductivity is a function of the water content in the membrane of the cell. Authors have different approaches on how to retrieve the water content. Abdin et al. (2015) suggests that the water uptake can be approximated. It is suggested to have a value of 0.5 for dry membrane conditions. When the membrane is exposed to water and saturated gas, water content should have a value between 12-14 and for liquid water it should have a value of 22. Ruuskanen et al. and Yigit and Selamet (2016) however suggests that the water content can be obtained by using a defined equation.

$$V_{ohm} = \frac{\delta}{\sigma} i_{cell} \tag{4}$$

3.1.2. Thermal model

The amount of generated heat from the stack can be determined by a thermal model, as Tiktak (2019), Fragiacomo and Genovese (2019) and García-Valverde et al. (2012) propose. When the electrolyzer is operating above the thermoneutral voltage (V_{th}), losses are generated in the form of heat.

The authors Tiktak, Fragiacomo and Genovese, and García-Valverde et al. suggest that these phenomena can be modeled with the lumped thermal capacitance method. These studies all use the same approach to model the thermal effect mathematically, where the temperature gradients within the electrolyzer stack are neglected. This means that the ambient temperature (T_a) is assumed to be static, and the temperature in the different electrolyzer components is uniform everywhere throughout the stack. These studies also assume that the Joule Effect is negligible.

For a lumped thermal capacitance model, the overall heat balance of the system is defined by the generated heat (Q_{gen}) minus the heat loss to the environment (Q_{loss}) and cooling (Q_{cool}). The lumped thermal capacitance (C_{th}) is the overall thermal capacity of the stack, which is there to simulate the thermal inertia of the system. This is important during dynamic conditions when fluctuations in the power output occur, for example as during start up time. This model can therefore be written as the following continuous dynamic equation:

$$C_{th} \frac{dT}{dt} = Q_{gen} - Q_{loss} - Q_{cool} \tag{5}$$

The authors of all mentioned studies use the same equation of determining the generated heat (Q_{gen}), where the difference between the total cell voltage and the thermoneutral voltage (V_{th}) make up for the heat generated in the cell. However, the calculation of the total heat losses (Q_{loss}) in the system differs between the authors. Fragiacomo and Genovese calculates the heat loss by assuming the total thermal resistance of the electrolyzer through a parameter R_t. However, the authors imply that the parameter is difficult to estimate as it is dependent on several variables, such as the size of and the materials used in the electrolyzer. Tiktak on the other hand, calculates the total heat loss by natural heat transfer i.e. convection and radiation from the stack. The design of the stack is simplified to a cube, where air convection losses are modelled as a low velocity air convection problem. The radiative heat losses are calculated by using the Stefan-Boltzmann constant and the coefficient for unpolished stainless steel.

3.1.3. Cooling circuit

There is a strong correlation between thermal management inside the stack and the overall performance of the PEM electrolyzer stack. This means that the stack needs to be cooled in to ensure optimal operation and durability in each cell of the stack. The kinetic reaction inside the cell is negatively affected if too much heat is removed. However, a cell temperature above its optimal temperature will cause the membrane to dry up which results in poor proton conductivity. This means that keeping the water content in the membrane is crucial in the stack management strategy. The cooling plate is therefore often put in between the cells to control the thermal conditions of the cells and will thus also keep uniform temperature throughout the stack. However, implementing such a cooling system increases the complexity, costs and weight of the system (Soupremanien et al., 2012).

The heat produced in the stack is extracted via a cooling medium that flows through the bipolar plates of each cell. According to Soupremanien et al. (2012), most of the PEM fuel cells are cooled with liquid. The liquid is usually de-ionized water, which is cheap, non-toxic and has a high heat capacity. Conversely, Tiktak (2019) warns that de-ionized water is a strong solvent for many harmful chemicals which may cause issues due to the water being circulated. Furthermore, water is an efficient cooling medium, but has its limits if operating in ambient temperatures below freezing. Sohn et al. (2005) suggest that air cooling could be used and would be a cheap way of keeping the system cool. However, the system is not able to be kept at a uniform temperature when increased above the low kW range.

For a liquid cooling system, Soupremanien et al. suggest that the thermal performance depends on three parameters: water content in the membrane, control of pressure drop inside the cooling system and uniform temperature in the cell to ensure electrochemical reactions and increased lifetime of the cells.

Tiktak proposes a cooling system similar to the calculations of Soupremanien et al. Tiktak's cooling channels are integrated in the bipolar plates, which are placed between the cells in the stack parallel to the process water. The channels are dimensioned for 1 mm in height and 1.5 mm in width. These cylindrical channels then flow in a straight line from one side of the stack to the other. This allows Tiktak's stack to have 79 cooling channels per cell. Furthermore, Tiktak suggests that large temperature differences in the cells leads to non-homogeneous loadings of the cell, since the ohmic resistance and activation overpotential are temperature-dependent. It is therefore recommended that the temperature difference should be kept below 10°C. High temperature gradients inside the stack increase the cell degradation and lead to faster cell ageing. Low temperature gradients inside the stack minimize cell degradation and reduce the cell aging.

3.2. Modeling Alkaline electrolyzer

Fragiacomo and Genovese (2019) have compared different modeling approaches for Alkaline electrolyzer. The Alkaline technology is more complex than for PEM but in general, the modeling approach is similar for both electrolyzers. The Alkaline model considers an electrochemical and thermodynamic part, just like for the PEM electrolyzer. Although one difference occurs in the chosen equations for the cell voltage in the electrochemical model. The authors found that the most convenient way of modeling the voltage is by using a simple approach based on empirical correlations, since too many parameters add a complexity to the model which creates difficulties to adapt it for different sizing's.

As previously mentioned in the *Modelling PEM Electrolyzer* section, the electrochemical model determines the cell voltage. The chosen empirical correlation of Fragiacomo and Genoveses (2019) model for cell voltage is based on a temperature dependent model by Ulleberg (2003). The r-values represent the ohmic overpotential, while the s- and t-values represent the activation overpotential.

$$V_{cell} = V_{rev} + (r_1 + r_2 * T) * i + (s_1 + s_2 * T + s_3 * T^2) * \log_{10}[\left(t_1 + \frac{t_2}{T} + \frac{t_3}{T^2}\right) * i + 1] \quad (6)$$

The thermal model for the alkaline electrolyzer similar to the PEM modelling procedure, which can be looked into in the *Modelling PEM Electrolyzer* chapter. A lumped thermal capacitance approach is a commonly used method and the overall energy balance is equal for both alkaline and PEM thermal models.

3.3. Heat pump

The purpose of a heat pump is to upgrade a low temperature heat source to a higher heat sink temperature by using a refrigerant. A heat pump is therefore a suitable unit for low-grade waste heat recovery, where the basic working principle is that heat is extracted from a low temperature heat source. Heat extraction from a heat source occurs when the refrigerant is evaporated, while the refrigerant must be at lower temperature than the heat source for this to occur. The evaporated refrigerant is then led into a compressor, which pressurizes and lifts the temperature of the refrigerant. Next, a condenser liquifies the refrigerant making it release the upgraded heat to the source of application. The refrigerant is then expanded through a valve before being led to an evaporator again (Granryd et al., 2009).

A common type of heat pump technology is the "basic vapor compression cycle" which consists of a single stage cycle. This construction is suitable for small temperature lifts. In the single stage compression cycle, the refrigerant is evaporated to saturated vapor. Isentropic compression then occurs, and the refrigerant is at saturated liquid state when leaving the condenser. At the evaporator and condenser, two isobaric heat exchanges follow. Before closing the cycle, an isenthalpic expansion takes place (Granryd et al., 2009).

When large temperature lifts are required, a two-stage heat pump cycle is a more suitable choice due to the increased efficiency of the heat pump. It follows the same working principle as the single-stage cycle, but it is often equipped with an additional compressor (Granryd et al., 2009). Granryd et al. suggests that a two-stage cycle should be used when the required temperature lift is higher than 50 °C. In a research paper, Hu et al. (2017) compare the performance of a single and multi-stage water-source heat pump (WSHP). Multi-stage WSHP includes a two-stage and three-stage compressor cycle. Schematics of the two-stage compressor cycle can be seen in Figure 9. WSHP provides higher energy efficiency and a higher temperature output when compared to air-source heat pumps. The authors conclude that a two-stage compression cycle with operating refrigerant R1234ze(Z) can lift temperatures from 50 °C to 120 °C. In comparison with a single stage compression cycle with the same refrigerant, the coefficient of performance (COP) value is 9.1 % higher. When evaluating the performance of all three cycles, the authors chose to model the systems for a constant waste heat input (420 kW) and a fixed output temperature (120 °C). The waste heat temperature source varied between 50-90 °C. Results of the study showed that the COP value for a single-stage, two-stage and three-stage cycle is 3.59, 3.93 and 4.18 respectively.

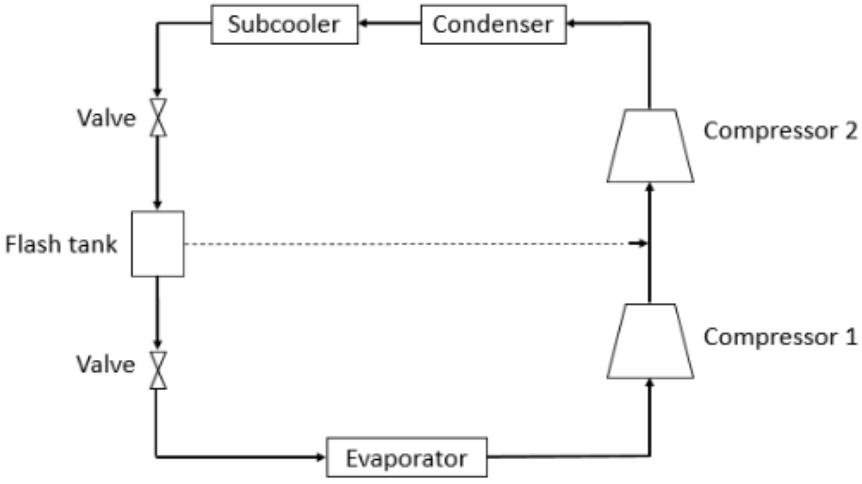

Figure 9. Two-stage compressor cycle presented and inspired by Hu et al. (2017)

A water-source heat pump is operating with two heat exchangers, with water circulating in each cycle. The first water cycle and heat exchanger are situated at the evaporator side of the heat pump. The water is heated up by a heat source, which then provides large enough heat to evaporate the refrigerant in the heat pump cycle. After the heat exchange at the evaporator side, the water is cooled down before it is heated up again by the heat source. The cycle is then repeated. At the condenser side of the heat pump, upgraded heat is transferred to the second heat exchange water cycle. See Figure 10 for illustration. The transferred heat can be injected into a district heating network, residential buildings, and other useful applications (Hepbasli et al., 2014).

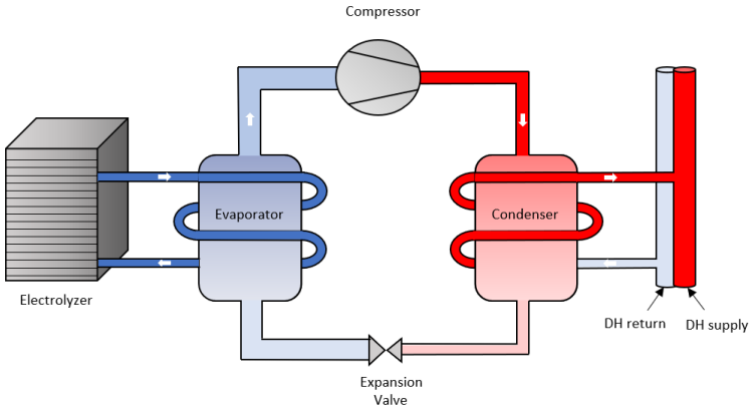

Figure 10. Schematics of heat pump connected to the electrolyzer and district heating network. Inspiration for illustration received from Ninikas et al. (2014).

3.3.1. Type of refrigerants

When choosing a suitable refrigerant for a heat pump, it is valuable to choose one with thermodynamic characteristics that is suitable for the heat pump of interest. A refrigerant with low boiling point should be chosen for low temperature heat sources, while refrigerants with higher boiling points are more appropriate for high temperatures heat sources. The potential environmental harm that can be caused by the refrigerant is also a factor that is important to consider. The Global Warming Potential (GWP) and Ozone Depletion Potential (ODP) are used to describe the environmental load of a refrigerant. A higher GWP and ODP value means that a refrigerant can cause a higher environmental harm in comparison with lower values, if leaked into the atmosphere (HTP IEA, n.d.).

Makhnatch (2014) writes that the number of reliable refrigerants is limited when designing a high temperature heat pump i.e., when heat over 75 °C is delivered. Previously commonly used refrigerants for medium and high temperature applications have been R500 and R114. However, they are now prohibited in terms of usage due to a high ODP. R134a, a more environmentally friendly alternative to R500, has now replaced the latter for medium temperature applications. A suitable replacement for R114 is R1234ze(Z) for high temperature applications according to Maknatch, since they share comparable thermodynamic properties. A study performed by Fukuda et al. (2014) also claims that R1234ze(Z) is a suitable heat pump refrigerant when temperatures are upgraded over 100 °C. Hu et al. (2017) account for the natural refrigerant ammonia, also denoted R717, as a medium with high boiling point and low environmental impact. The drawback with R717 is however the toxicity of the refrigerant. Due to R1234ze(Z) still having more suitable thermodynamic characteristics and being less dangerous in comparison with the R717, Hu et al. also propose the use of R1234ze(Z) as refrigerant for high temperature applications. A comparison between the environmental impacts of the refrigerants R134a, R1234ze(Z) and R717 can be seen in Table 1.

Table 1. Characteristics of refrigerants for high temperature applications (Linde, n.d.).

	R134a	R1234ze(Z)	R717
GWP	1300	7	0
ODP	0	0	0
Toxic	No	No	Yes

3.3.2. District heating networks and integration of heat pumps

There are four generations of district heating (DH) technologies (Lund et al., 2014), however, the first and second generation are not used in Sweden due to the existing up-to-date alternatives. The third generation is instead the most common DH technology (Werner, 2017) while the fourth generation of DH has not yet been implemented for use in Sweden (Lund et al., 2014).

For third generation of DH networks, pressurized water is used as an energy carrier with supply temperatures under 100 °C (Lund et al., 2014). In Sweden however, the supply temperature is correlated with the outdoor temperature. Lower outdoor temperatures require higher supply temperatures – which can be over 100 °C during winter periods (Werner, 2017). When integrating low-temperature waste heat into the third generation of DH-network, upgrading technologies like heat pumps are often required due to the high operating temperatures. The integrated heat pump will only be able to deliver a part of the required heat of the system (Sayegh et al., 2018).

While the third generation of DH technology is mainly used in Scandinavia to this day, the future of the fourth generation of DH networks is evolving. Fourth generation of DH networks also use pressurized water as an energy carrier, but with lower supply temperatures. This operational parameter is envisioned to enable easier and more cost-effective integration of low-temperature waste heat into a DH network (Lund et al., 2014). This is because greater possibilities to integrate heat pumps will be offered, but also because it enables a better match for waste heat and supply temperatures. In some cases, this means that the use of a heat pump may not even be necessary (Sayegh et al., 2018).

Heat pumps is a commonly used technology within DH-networks, and it have been used in Swedish grids since 1980. During the years 1981-1985, a total capacity of 1215 MW was installed and 80 % of the installed capacity is still in operation 30 years later. The expansion of heat pumps during the 1980´s was due to an abundance of power from nuclear generation. In the future it is although expected that heat pumps in the DH-networks will fulfil the purpose of providing flexibility and lower environmental impacts (Averfalk et al., 2017). Heat pumps can provide several advantages when integrated into a district heating network. According to Geyer et al. (2020) heat pumps are able to provide more flexibility to the grid, increase the use of heat generation from renewable energy sources and allow for lower supply temperatures in the grid. Flexibility is offered by the enlarged choice of heat sources that can be implemented into the grid, by upgrading in a heat pump. Lower supply temperatures are feasible since the

heat can be increased at points where there is a demand in the grid, thus reducing the overall heat loss in the network as well.

In the study of Geyer et al. (2020) the authors explain that studies show that heat pumps can improve the third generation of DH networks – if waste heat sources are available for integration. The improvement concerns fuel efficiency and flexibility of the network. In fact, if a significant amount of abundant excess heat is recovered, it could reduce or even replace the need for fueled boilers in some scenarios. In a study by Wahlroos et al. the authors also conclude that the utilization hours of a heat boiler decreased when waste heat from a data center was utilized in the DH network. David et al. (2017) mentions a similar example for waste heat recovery but for Stockholm, Sweden, where a heat pump of an installed capacity of 230 MW recovers the low-grade heat from sewage water. The DH grid in Stockholm has benefited from this utilized heat, and the authors imply that similar solutions can be applied to benefit the DH network in other cities as well. The greatest characteristics of waste heat from sewage water is the high temperature of the heat, supply stability and proximity to urban areas. Other heat sources with similar characteristics could therefore replace sewage water, while receiving similar grid benefits.

Integration of heat pumps into the DH network can be performed in multiple ways. Geyer et al. (2020) however explains that in a case where an external heat source is integrated into a DH network i.e., waste heat, it can either be integrated in parallel or in series to the DH supply side (see Figure 11). In a case where the heat pump is coupled in parallel, the DH return side is the inlet stream to the condenser while the outlet stream is coupled to the DH supply side. If the heat pump is coupled in series, then the condenser will just heat up the supply side of the DH network. The coupling of heat pump is a choice of preference and purpose of the heat recovery. Neither parallel or serial type of coupling does however affect the operation of an existing heat generation plant.

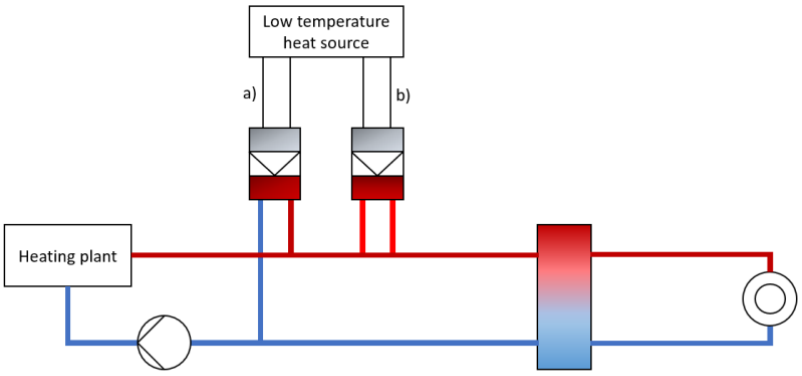

Figure 11. Integration of heat pump on the DH-network with parallel (a) and serial (b) connection. Inspiration for illustration received from Geyer et al. (2020).

3.4. Economic assessment of waste heat recovery on DH-networks

According to Wahlroos et al. (2017), and in line with the considerations above, it can be beneficial for DH operators to buy waste heat. If the waste heat is a reliable heat supply, it could reduce the need of peak production of heat. This peak is often produced by fossil fuels – thus it has the ability to reduce the production costs and environmental impact. However, it is worth mentioning that DH operators must comply under incentive that waste heat can only be bought for heating supply if it is the more cost-effective choice in comparison to the conventional fuel that is used for heat supply. This means that the DH operators can only benefit from the waste heat if it is cost competitive. Since heat pumps is a common alternative for waste heat upgradation, Averfalk et al. (2017) further claims that large heat pumps also compete with biomass CHP plants in terms of cost efficiency. For Swedish market conditions, heat pumps are more competitive at lower electricity prices. However, if the electricity prices within a market is volatile, it is preferable to use both heat pumps and CHP plants for heat generation in a DH-network (Averfalk et al., 2017).

Another factor that impacts the price competitiveness of waste heat is the investment cost of a heat pump, which is largely dependent on the used heat source according to Pieper et al. (2018). Heat pumps that use reliable heat sources like sewage water becomes more profitable with larger capacities due to a constant heat source investment cost, in comparison to heat sources with an inconsistent cost. The authors also conclude that heat pumps that performs a higher temperature lift between the heat source and heat sink are generally costlier as well. However, these findings were applied to heat pumps using natural refrigerants such as ammonia and carbon dioxide.

A comparison of LCOH costs for different DH thermal energy sources is presented in Table 2. The compared energy sources are waste fueled CHP-plant, wood chip fueled CHP, biomass boiler, gas turbine and electric boiler. The LCOH-calculations are based on technical and economic factors for a German energy system, such as system efficiencies, system costs, economic lifetimes, fuel prices and CO_2 prices which are all connected to the cost of operating the heat. Costs for DH pipes are however excluded from the calculations (Hansen, 2019).

Table 2. LCOH costs for different thermal energy sources (Hansen, 2019).

	Waste CHP	**Wood-chips CHP**	**Boiler (biomass)**	**Gas turbine**	**Electric boiler**
LCOH cost [SEK/kWh]	0.43	0.43	0.43	0.32	0.32

4. CURRENT STUDY

This chapter demonstrates the methodology for developing the model of the proposed system in depth. The approach and approximations used for the economical evaluation is also clarified. The model consists of an electrolyzer (modelled for both PEM and alkaline), heat pump and heat exchanger. An electrical pump was also dimensioned to calculate the electrical costs of the system. Electrolyzer and heat pump validations are also included in this chapter.

4.1. Modelling PEM Electrolyzer

The PEM electrolyzer model consists of an electrochemical, thermal, and cooling part. The electrochemical and thermal parts are modelled for one static cell, which enables the model to be scaled up to meet the capacity requirement of 100 MW. The cooling model is presented in section 4.3 and is modelled over the course of one year. When referring to the temperature of the cell (T_{cell}), it is assumed to be the highest temperature in the cell. In reality, the temperature in the cell is not uniform.

4.1.1. Electrochemical model

The electrochemical model illustrates the electrochemical properties of a single cell. Performance of the cell is determined by the cell voltage, which is dependent on the current density and temperature inside the cell. The cell voltage is calculated from Equation 1. The required number of cells needed to meet the required power (P) of the stack is calculated by using the current density (i), calculated cell voltage and the assumed cell area (A_{cell}):

$$N_c = \frac{P}{V_{cell} * i * A_{cell}} \tag{7}$$

The total stack voltage is then received by multiplying the cell voltage with the number of cells required to reach the installed power capacity.

4.1.1.1. Open circuit voltage

The open circuit voltage is calculated with Equation 2, previously presented in section 3.1.1. The partial pressure for water, P_{H2O}, is assumed to be 1. Reversible cell voltage (V_{rev}) is defined as a function of the cell temperature. The reversible voltage is the lowest voltage that is needed in order for water to decompose (Falcão & Pinto, 2020):

$$V_{rev} = 1.229 - 0.9 * 10^{-3}(T_{el} - 298)\ [V] \tag{8}$$

According to Fragiacomo and Genovese (2019), the partial pressures of the hydrogen and oxygen can be expressed by the ideal gas equation (eq. 9a and 9b). Oxygen is only produced at

the anode while hydrogen is produced at the cathode side of the electrolyzer. Hence, the volumes of the anodic (Vo_{an}) and cathodic (Vo_{ca}) chambers are both assumed to be 0.01 cm^3.

$$p_{H_2} = \frac{RT_{cell}}{Vo_{ca}} \dot{n}_{H_2} \quad (9a)$$

$$p_{O_2} = \frac{RT_{cell}}{Vo_{an}} \dot{n}_{O_2} \quad (9b)$$

According to Faraday's law, the hydrogen production rate in an electrolyzer is linear to the electric charge that is transferred at the electrodes (Olivier et al., 2017). The hydrogen production is described in Equation 10a, which is defined as a function of the current (I) and the number of free electrons that are transferred in the reaction (z = 2). Finally, Faraday efficiency ($\eta_{Faraday}$ = 0.99) is introduced as a constant to describe electron losses due to leakage current and parasitic currents (Fragiacomo & Genovese, 2019). Regarding the oxygen, Fragiacomo and Genovese suggests that the production of oxygen is 50 percent less than the hydrogen production, as can be seen in equation 10b.

$$\dot{n}_{H_2,p} = \eta_{faraday} \frac{I}{zF} \quad (10a)$$

$$\dot{n}_{O_2,p} = \frac{1}{2} \dot{n}_{H_2} \quad (10b)$$

4.1.1.2. Activation overpotential

The Butler-Volmer equation presented in section 3.1.1 defines the activation overpotential in Equation 3. The values of the exchange current density (i_o) and charge transfer coefficient (α) can affect the outcome of the activation overpotential greatly. Both Fragiacomo and Genovese (2019) and Tiktak (2019) use a charge transfer coefficient of 0.5, with the assumption that the charge distribution is in symmetry. This value is therefore implemented into the model by using the same assumption. The exchange current density depends on various factors, some of them are the electrocatalyst, electrodes and cell temperature. These parameters are considered as confidential for which the manufacturers are oftentimes unwilling to share information of. However, the exchange current density can be modelled and curve-fitted for by using an Arrhenius expression (García-Valverde et al., 2012):

$$i_0 = i_{0,ref} * e^{-\frac{E_{act}}{R} * \left(\left(\frac{1}{T}\right) - \left(\frac{1}{T_{ref}}\right)\right)} \; [A] \quad (11)$$

where $i_{o,ref}$ is the reference value of exchange current density at the reference temperature T_{ref}, and E_{act} is the activation energy for the anode and cathode. The used parameter values can be seen in Table 3.

4.1.1.3. Ohmic overpotential

The ohmic overpotential is defined by electronic and ionic losses. Electronic losses are small in comparison to the ionic losses thus, they are assumed to be negligible. The ionic losses are caused by the flow of ions in the membrane and are highly connected to the resistance of the material. The ohmic overpotential therefore is defined in Equation 4 in section 3.1.1. and it depends on the thickness of the membrane (δ) in centimetres and the conductivity of the material (σ). The material conductivity is expressed by Equation 12 below, where T is the electrolyzer temperature and λ is the membrane water content (Yigit & Selamet, 2016):

$$\sigma = (0.005139\lambda - 0.00326) * e^{1268*\left(\left(\frac{1}{303}\right)-\left(\frac{1}{T}\right)\right)} \left[\frac{S}{cm}\right] \quad (12)$$

4.1.2. PEM electrochemical model validation

The electrochemical model is validated against the results from the study of Tiktak (2019), since the modelling methodology of the activation and ohmic overpotential has been used as a reference for this model. Assumptions from the reference study can be seen in Table 3.

Table 3. Used assumptions for validation of the PEM electrochemical model.

Variable	Symbol	Value
Charge transfer coefficient anode	α_{an}	0.5
Charge transfer coefficient cathode	α_{cat}	0.5
Exchange current anode	io_{an}	10^{-4} A/cm2
Exchange current cathode	io_{cat}	$0.75*10^{-3}$ A/cm2
Reference temperature	T_{ref}	318 K
Activation energy anode	$Eact_{an}$	90 000 J/mol
Activation energy cathode	$Eact_{cat}$	30 000 J/mol
Membrane water content	λ	14
Membrane thickness	δ	125 µm

The open circuit voltage calculations were not comprehensively presented in the study by Tiktak (2019). The partial pressures were therefore calculated by using an approach from Fragiacomo and Genovese (2019). However, Fragiacomo and Genovese did not present their results of the open circuit voltage. Due to this, the open circuit voltage is therefore validated against the results from Tiktak. According to Tiktak's results, the open-circuit voltage is 1.2474 V at 80 °C and 1.5 A/cm², whilst the result for this study displays 1.35 V for similar conditions.

The activation overpotential is compared against the results from Tiktak (2019) in Figure 12, for the same cell temperature of 80 °C but for different current densities. The values from the two compared models show very similar results, with only small deviations at higher current densities.

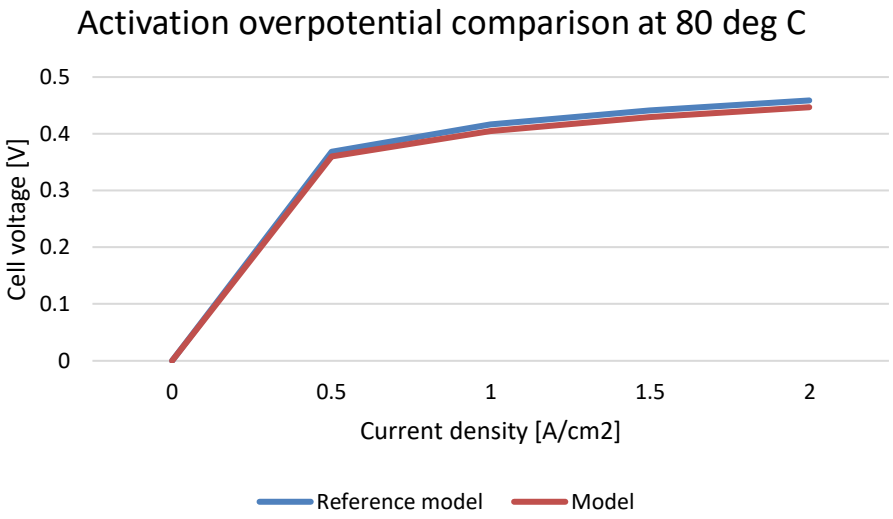

Figure 12. Activation overpotential as a function of temperature and current density, compared with the reference model by Tiktak (2019).

The ohmic overpotential deviates from the results of Tiktak (2019), as can be seen in Figure 13. Therefore, it is of necessity to emphasize that Tiktak regarded both the electronic and ionic resistance when calculating the ohmic overpotential - while the electrical resistance in the current collector and bipolar plate is neglected in this study. It is reasonable to assume that the deviation occurs due to this, which results in ~0.1 V lower difference in comparison to the reference study at 2.1 A/cm² and 10 °C.

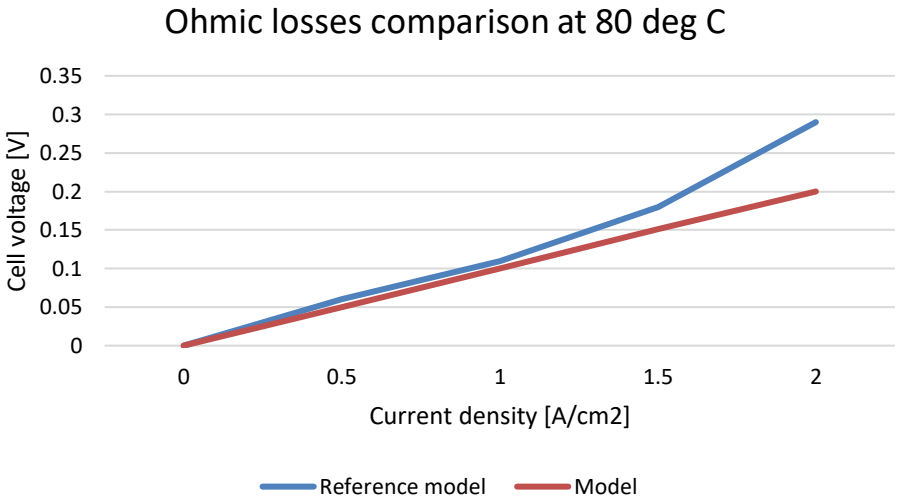

Figure 13. Ohmic losses as a function of temperature and current density, compared with the reference model by Tiktak (2019).

The calculated cell voltage for this study is mainly based of the modeling approach by Tiktak (2019), with an exception for the open circuit voltage calculation as previously mentioned. The accuracy of the electrochemical model validation is therefore further increased by comparing the results against other reference studies. This comparison is presented in Table 4. The reference studies in Table 4 are utilizing different current densities and cell temperatures, which is why the reference results for the cell voltage differ. However, the operational conditions of the reference models (i.e., temperature and voltage) are implemented into the developed model for this case study, and the error between the compared models are presented. The resulting deviation between the models is a result of applying different assumptions and approaches. However, the values of the electrochemical model are in-between the values of the reference studies, which may point to the fact that the results of this study are within an acceptable interval.

Table 4. A comparison of the results for the calculated cell voltage from this study and reference studies.

Studies	Applied temperature [°C]	Applied current density [A/cm²]	Reference results [V]	Results from this study [V]	Error [%]
Fragiacomo & Genovese (2019)	80	1.35	1.98	1.9	-3.99
Tiktak (2019)	80	1.5	1.82	1.93	6.04
Yigit et al. (2016)	70	0.6	1.7	1.79	5.81
Abdin et al. (2015)	40	0.6	1.99	1.91	-4.02

4.1.3. PEM Thermal model

The thermal model was developed by an approach from the study of Tiktak (2019) and García-Valverde et al. (2012).The thermal capacity (C_{th}) of the stack introduced by García Valverde et al. is stated in equation 5. The equation aims to explain the thermal inertia of the system, where the different components cool down and heat up differently.

$$C_{th}\frac{dT}{dt} = Q_{gen} - Q_{loss} - Q_{cool} \quad (5)$$

However, the electrochemical and thermal model in this study is developed for steady state conditions. This means that the electrolyzer is assumed to be operating 24 hours per day, without start-ups and stops. Therefore, the thermal inertia of the system is not of interest. The useful generated heat can thus be simplified:

$$Q_{useful} = Q_{gen} - Q_{loss} \quad (13)$$

where the generated heat from the electrolyzer in operation can be defined from the thermal balance given by García-Valverde et al. (2012):

$$Q_{gen} = n_c(V_{cell} - V_{tn}) * i * A_{cell} \quad (14)$$

In order to determine the useful generated heat, heat losses to the environment must be calculated. These heat losses occur by convection and radiation from the material to the environment. The heat loss is introduced by Tiktak where A_{stack} is the surface area of the stack, T_s is the surface temperature of the material, T_{amb} is the ambient temperature, h_c is the convective heat transfer and h_r is the radiative heat transfer coefficient:

$$Q_{loss} = (h_c + h_r) * A_{stack} * (T_s - T_{amb}) \quad (15)$$

The geometry of the stack is assumed to be a cuboid, as illustrated in Figure 14. The length and width of each cell is 31.7 cm, and the height is 0.44 cm. The cells are stacked upon each other, creating an electrolyzer stack and total surface area of 191.8 m².

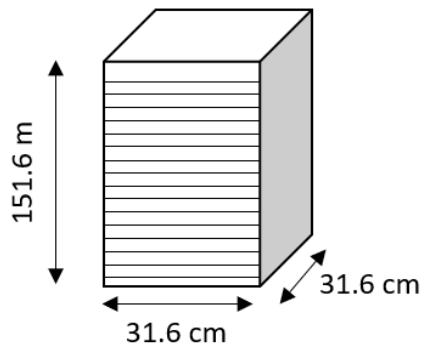

Figure 14. Dimensions of the PEM electrolyzer stack.

The radiative heat transfer coefficient in equation 16a is defined by the emittance factor of the unpolished steel ($\varepsilon = 0.6$), Stefan-Boltzmann constant ($\sigma = 5.670 * 10^{-8}$) and the mean stack surface temperature (T_{stack}). Furthermore, the convective heat transfer coefficient in equation 16b is expressed as by the Nusselt number (Nu), thermal conductivity (k) and length of the stack (L).

$$h_r = 4\varepsilon\sigma {T_{stack}}^3 \left[\frac{W}{m^2K}\right] \quad (16a)$$

$$h_c = \frac{\overline{Nu}*k}{L} \left[\frac{W}{m^2K}\right] \quad (16b)$$

When choosing the appropriate equation for the Nusselt number, the flow type needs to be determined by the Reynolds number. Reynolds number is defined by the ambient air flow (V_{amb}), length of the stack (L) and the kinematic viscosity for air (ν) (Technologies, n.d.). The flow type will determine the choice of the Nusselt number.

$$Re = \frac{V_{amb}*L}{\nu} \quad (17)$$

A slow-moving air flow is assumed in this study (v = 0.2 m/s, υ =1.516*10^{-6}, Re ~4200), meaning that the air flow through the electrolyzer is laminar. This will require a Nusselt number for laminar flow (Incropera et al., 2013) where Pr is the Prandtl Number and assumed to be 0.73:

$$\overline{Nu} = 0.664 * Re^{\frac{1}{2}} * Pr^{\frac{1}{3}} \quad (18)$$

4.1.4. PEM thermal model validation

The thermal model is developed by using a similar approach as Tiktak (2019). Tiktak´s modelling approach is therefore used as a reference when validating the thermal model. However, Tiktak utilizes a slightly different equation to calculate the Nusselt number:

$$\overline{Nu} = 0.66 Re^{0.675} Pr^{1/3}$$

Assuming slow moving air, the reference study calculates that the Nusselt number should be 184 while assuming an ambient air temperature of 10 °C. A comparison of the calculated Nusselt number, convective and radiative heat transfer as well as the thermal heat losses are presented in Table 5. A slight deviation can be seen for the radiative heat loss – even if equal parameter values was used for the temperature and emittance factor. This deviation is most likely due to a rounding difference in the Stefan-Boltzmann constant. The rounding difference causes the anomaly in overall heat loss; however, it is a small alteration which is determined to be negligible.

Table 5. Parameters used for validation of the PEM thermal model.

Parameter	Reference study	Current study
Ambient temperature [°C]	10	10
Stack area [m]	0.75	0.75
Nusselt number	184	184
h_c [W/m2, K]	14.6	14.6
h_r [W/m2, K]	4.36	4.37
Q_{loss} [W]	998.9	1000.1

The generated heat is calculated by Equation 14 which is a function of the cell voltage (V_{cell}), thermoneutral voltage (V_{th}), current density and cell area. The cell voltage has already been validated in chapter 4.1.2 and the thermoneutral voltage is 1.481 V at standard conditions. Therefore, there is no need to validate the heat loss calculation further.

4.1.5. Operational conditions of PEM electrolyzer

This study aims to create an electrolyzer model which as closely as possible resembles a modern commercial large-scale PEM electrolyzer. Tiktak (2019) suggests that a current density of 1.5 A/ cm^2 at ~80 % efficiency is a common used operational parameter. Furthermore, Fragiacomo and Genovese (2019) states that the commercialized modern PEM electrolyzers utilize 80 °C as an operational cell temperature. The suggested values are therefore implemented in the PEM electrolyzer model.

Pressures are set to 5 bar at the anode and 30 bar at the cathode for the PEM electrolyzer. Lower pressures at the anode results in a higher production of water vapour in the product flows, which leads to lost heat. Heat losses are thus mitigated at higher pressures such as 5 bar in the anode (Tiktak, 2019).

4.2. Modelling alkaline electrolyzer

The alkaline electrolyzer model consists of an electrochemical, thermal and cooling part, as for the PEM model. A similar modelling approach is followed for the alkaline model, although, the electrochemical and thermal model are based on different equations. The cooling model presented in section 4.3 is applied to both electrolyzers.

4.2.1. Alkaline electrochemical model

The alkaline electrolysis technology is more complex compared to PEM technology. Because of this complexity, empirical correlations are often used when alkaline electrolyzers are modelled (Fragiacomo & Genovese, 2019). The cell voltage in this study is therefore expressed by an empirical equation (Equation 6, presented in section 3.2) retrieved from the study by Ulleberg (2003). The reversible voltage (V_{rev}) is calculated by Equation 8. The values for the r, s and t parameters are retrieved from Ulleberg and can be found in Table 6.

Table 6. Parameters used to calculate the alkaline cell voltage presented in Eq. 6.

Parameter	Value
r1	0.0004296 [Ohm m²]
r2	-4.153*10-7 [Ohm m²/k]
s1	0.1803 [V]
s2	0 [V/K]
s3	0 [V/K]
t1	0.05171 [m²/A]
t2	-2.415 [m²/A, K]
t3	8134 [m²/A, K²]

The empirical equation used to describe the electrochemical model is a commonly suggested equation throughout literature, due to its accuracy and adaptability to different electrolyzers. It is a trustworthy equation, and will therefore not be validated further in this study than it already has been through various peer-reviewed articles.

4.2.2. Alkaline Thermal model

The alkaline thermal model is like the PEM thermal model, where equation 13 is used to describe the energy balance in the stack and equation 14 is utilized to calculate the generated heat. Ideally, the same calculation approach for heat losses would therefore be used as for the PEM thermal model. However, essential measurement data for the stack dimensions could not be found. Therefore, the heat loss is expressed empirically using the following equation:

$$Q_{loss} = \frac{1}{R_t}(T_{cell} - T_{amb})\ [W] \quad (19)$$

where the ambient temperature ($T_{ambient}$) is constant at 20 °C and the total thermal resistance of the electrolyzer (Rt) is assumed to be 0.167 °C/W (Fragiacomo & Genovese, 2019). The

thermal resistance of the alkaline electrolyzer show significant deviations due to improvements in the technology over time. Recent literature however suggests that a thermal resistance of 0.167 °C/W should be used, which is therefore applied for this study.

4.2.3. Operational conditions of Alkaline model

Fragiacomo and Genovese (2019) suggest that the nominal operating temperature of a modern commercial alkaline electrolyzer is 80 °C. The cell area is assumed to be 2082 cm^2. Furthermore, the authors utilize an operating current of 200 A that is also validated towards experimental data. These parameters are chosen for the aim of producing 180 kg hydrogen per day – to keep up with standards that are set by California Fuel Cell Partnership. The chosen parameters for the modelled alkaline electrolyzer in this study are therefore identical with the choice of Fragiacomo and Genovese, as it is deemed that it will produce results that are reasonable with modern commercial alkaline electrolyzers.

There may exist alkaline electrolyzers that produce hydrogen in a more efficient manner, however, it will not be analysed further as it is beyond the scope of this study.

4.3. Cooling circuit design for PEM and Alkaline

A cooling circuit is developed to fulfil two functions i.e., to cool the electrolyzer stack while extracting the heat and to simultaneously provide the extracted heat to an upgrading unit. The cooling circuit is therefore designed as a closed loop system with liquid water as cooling medium, as can be seen in Figure 15. The operating cell temperature of both PEM and Alkaline electrolyzers are set to 80 °C due to efficiency and operational matters. According to Soupremanien et al. (2012), cooling of the electrolyzer is crucial to preserve an optimal cell temperature, which increases cell effectiveness and lifetime. Heat is extracted from the electrolyzer via small channels inside the electrolyzer and the outlet temperature of the heated water is 79-80 °C. This extracted heat will be referred as waste heat in this study.

When comparing the waste heat temperature to the required supply temperatures in the DH-network, the waste heat temperature is sufficient during the summer periods. However, the temperature is not high enough for the fall, winter and spring periods. The waste heat therefore needs to be increased to match the highest supply temperature in the DH-network, which is over 100 °C. For this specific case, a high-temperature heat pump is chosen as a heat upgrading unit. Also, the heat pump is integrated on the DH-network by parallel coupling presented in Figure 11.

The waste heat from the electrolyzer will be brought to the heat pump where heat exchange occurs, which cools down the waste heat to 74-75 °C. This process is then continuedly repeated to preserve the electrolyzer stack temperature at 80 °C. An electrical pump should preferably be used to circulate the water throughout the cooling circuit.

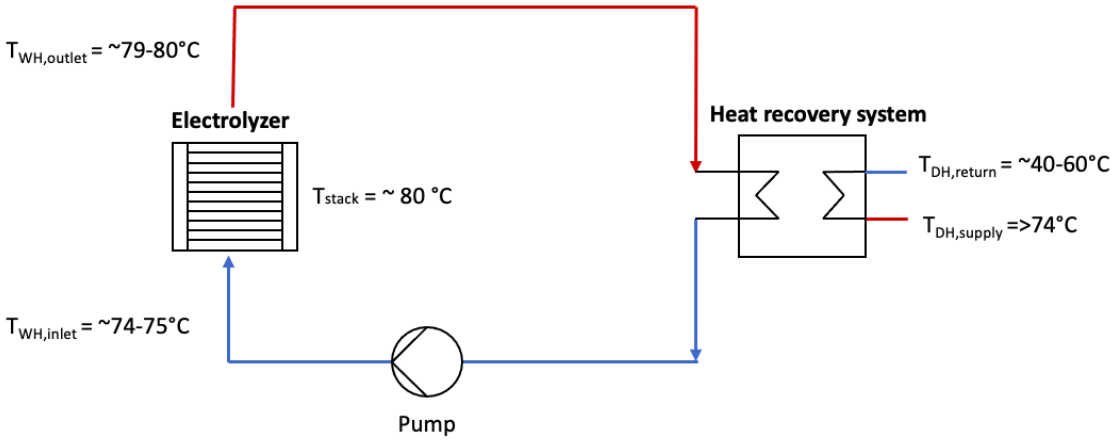

Figure 15. Closed-loop cooling system.

4.3.1. Heat extraction from electrolyzer

Tiktak (2019) proposed a cooling system for a PEM electrolyzer, where heat is extracted from each cell in the stack by small channels that are drilled into the bipolar plate. The channels are 1 mm in height and 1.5 mm in width in which cooling fluid i.e., liquid water, cross the cell from one side of the stack to the other. Tiktak further suggests that 79 channels per cell should be drilled. There is a lack of similar studies for Alkaline electrolyzers. The recommended cooling design for PEM will therefore be the foundation of the cooling system in this study, for both PEM and Alkaline electrolyzers. However, the modelling of the heat extraction will be further simplified from Tiktak´s approach; the electrolyzer will be considered as a heat source that is connected to a separate heat exchanger. The Alkaline cooling system is assumed to have identical cooling channel measurements as for the PEM electrolyzer. Although, the Alkaline cell area is larger, but the ratio of cooling channel-to-area will remain similar to PEM. This means that the alkaline cell needs 114 cooling channels when the same ratio is considered.

The energy balance from equation 14 calculates the amount of thermal energy that is possible to extract from the stack. This heat is therefore equal to the amount of energy that can be used to cool the system:

$$Q_{cool} = Q_{useful}$$

A specific mass flow of the cooling fluid is required to extract all available excess heat from the electrolyzer stack. According to Tiktak, a small temperature change of approximately 5 °C in the cooling fluid is essential to maintain the electrolyzer in optimal functioning conditions. However, due to the relatively small temperature difference, a higher mass flow will be necessary for the cooling system. The mass flow is expressed by the equation below, where the temperature difference (ΔT_{cool}) is assumed to be 5 degrees:

$$\dot{m}_{cool} = \frac{Q_{cool}}{Cp_{co} * \Delta T_{cool}} \left[\frac{kg}{s}\right] \quad (20)$$

As the heat extraction is assumed to take place in a heat exchanger, it is calculated using the NTU-method:

$$Q_{cool} = \varepsilon C_{min}(T_{co} - T_{ci}) \ [W] \quad (21)$$

The effectiveness of the heat exchanger (ε) is the ratio between the maximum and real heat transfer rate. It is expressed as a dimensionless quantity and calculated as:

$$\varepsilon = 1 - e^{-NTU} \quad (22)$$

where NTU is given by the equation below. According to Tiktak (2019), the overall heat transfer coefficient (U) of the PEM electrolyzer is 1975 W/m², K. The overall heat transfer coefficient is considered to be identical for the alkaline electrolyzer. The heat exchanger area (A) is calculated using the mentioned cell dimensions, where the length of the PEM cell is 31.6 cm.

$$NTU = \frac{UA}{C_{min}} \quad (23)$$

and finally, where C_{min} is expressed by:

$$C_{min} = \dot{m}_{cool} * Cp_{cool} \quad (24)$$

The inlet (T_{ci}) and outlet (T_{co}) temperature of the cooling fluid is calculated to make sure that the temperature difference is 5 °C. The operational cell temperature (T_{cell}) is set to 80 °C.

$$T_{c,i} = T_{cell} - \frac{Q_{co}}{\varepsilon C_{min}} \ [°C] \quad (25a)$$

$$T_{c,o} = T_{c,i} + \Delta T_{cool} \ [°C] \quad (25b)$$

dTx will be used as a means to analyse the difference between the cell temperature and outlet cooling fluid temperature:

$$dT_x = T_{cell} - T_{c,o} \ [°C] \quad (26)$$

4.4. Heat pump design

According to the study by Hu et al. (2017), a high temperature heat pump with two-stage compressor had a 9.1 % higher COP ratio in comparison to a one-stage compressor. This result concerns a temperature increase of waste heat from 60-90 °C to 120 °C. The waste heat temperature from PEM and Alkaline electrolyzers are 79 and 80 °C respectively, while the highest required supply temperature in the DH-network is over 100 °C. The temperature interval in this study therefore corresponds well to the investigated one in the model by Hu et al. A high temperature heat pump with a two-stage compressor will therefore be modelled according to the proposed modelling approach by Hu et al. The heat pump will be used during hours when the supply temperature in the DH-network surpasses the waste heat temperature from the electrolyzer.

The heat pump is illustrated in Figure 16 and consists of two compressor stages that are divided by a flash tank. The flash tank separates the refrigerant into saturated steam and liquid; the steam is injected into a mixing chamber between the compressor stages while the liquid is brought to valve located ahead of the evaporator. A subcooler is combined with the condenser to supercool the refrigerant by 20 °C, this is to make sure that the refrigerant is in saturated liquid form. When choosing an appropriate refrigerant for the heat pump, it is vital that it is suitable for the required temperature lift as it affects the COP-value of the system. The refrigerant R1234ze(Z) was therefore chosen as it is suitable for the required operating conditions, and because of its low GWP value.

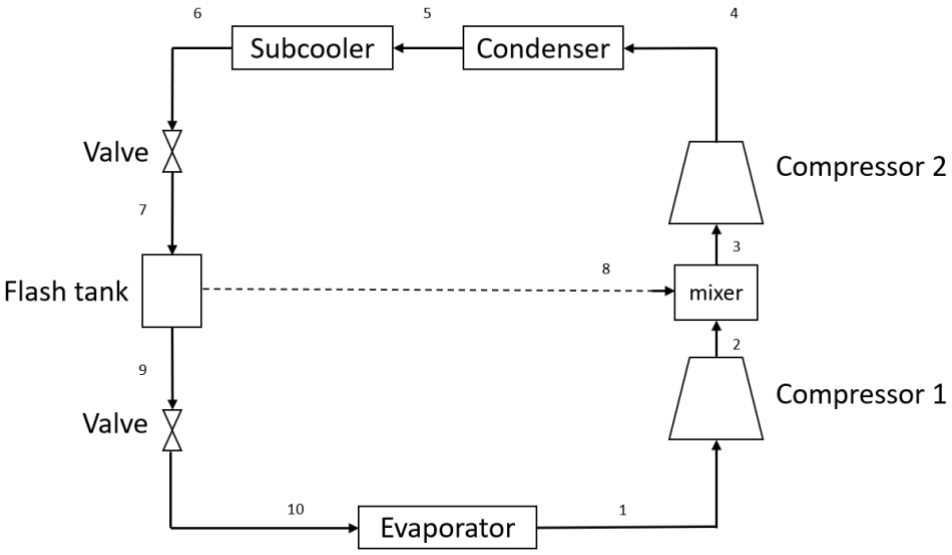

Figure 16. Two-stage compressor high temperature heat pump.

The heat pump was modelled with assumptions from the study by Hu et al. (2017). The pressure drops in the heat exchangers are neglected, and the expansion process is assumed to be isenthalpic, meaning that there is no enthalpy change in the valves. Further assumptions are listed in Table 7 below.

Table 7. Used assumptions for the heat pump.

Parameter	Symbol	Value
Condensing temperature [°C]	T_c	T_{supply} + 5
Evaporating temperature [°C]	T_{evap}	T_{ww} - 10
Isentropic efficiency [%]	η_{is}	70
Degree of subcooling [°C]	SC	20
Degree of superheating [°C]	SH	5

When modelling the heat pump, it is essential to find the COP-value, generated heat ($P_{th,out}$), compressor work ($W_{c,tot}$) and system efficiency ($\eta_{HP,sys}$). To receive these values, enthalpies and temperatures must be found for every point in the heat pump schematic (see Figure 16). The inlet and outlet temperatures and pressures of the evaporator are known i.e., point 1 and 10, which allows for the enthalpies to be calculated. The amount of waste heat (Q_{in}) that must be upgraded is retrieved from the electrolyzer model, which further allows for an energy balance of the evaporator to be conducted. The mass flow of the refrigerant in the first stage of the heat pump is therefore expressed as:

$$\dot{m}_1 = \dot{m}_{cool} * \frac{H_{in,ww} - H_{out,ww}}{(H_{10} - H_1)} \quad \left[\frac{kg}{s}\right] \tag{27}$$

The intermediate pressure (P_{in}) is the pressure between the compressor steps in point 2, and it is one factor that has a large impact on the COP value of the heat pump. The value of the intermediate pressure was not clarified by Hu et al. (2017), hence it is initially guessed to be at different values between the lower pressure (P_{low}) at point 1 and higher pressure (P_{high}) at point 4 in the heat pump schematic. The intermediate pressure is thereafter optimized for the supply and return side temperatures of the DH-network, as there is a correlation between DH temperatures and the intermediate pressure. When the intermediate pressure is known, the enthalpy after the first compressor stage can be found since the isentropic enthalpy (H_s) is a function of the intermediate pressure and the entropy.

$$S_1 = S_2$$

$$H_{2,s} \rightarrow S_2, P_2$$

$$H_2 = H_1 + \frac{H_{2,s} - H_1}{\eta_{is}} \quad \left[\frac{kJ}{kg}\right] \tag{28}$$

As previously mentioned, a compound of saturated liquid and vapor is injected into the flash chamber where it is then separated into two separate fluids. Saturated vapor is passed to the mixing chamber, where it is mixed with the superheated vapor from the first compressor stage.

The enthalpy before the second compressor (in point 3) is therefore affected by the quality of the refrigerant (X7) after the throttling process in point 7. Thus, the enthalpy in point 3 is defined by the quality of the refrigerant and the percentage of liquid going through the evaporator (1 - X7):

$$H_3 = (1 - X_7) * H_2 + X_7 * H_8 \ [\frac{kJ}{kg}] \quad (29a)$$

$$X_7 = \frac{H_7 - H_{sat,liq}}{H_{sat,vap} - H_{sat,liq}} \quad (29b)$$

The total required mass flow of the refrigerant ($\dot{m}_{tot}$) can now be calculated. The total mass flow of refrigerant allows for calculation of mass flow from the DH-network ($\dot{m}_{dh}$), required for utilizing the generated heat from the heat pump.

$$\dot{m}_{tot} = \frac{\dot{m}_1}{1 - X_7} \ \left[\frac{kg}{s}\right] \quad (30a)$$

$$\dot{m}_{dh} = \dot{m}_{tot} * \frac{(H_4 - H_5) + (H_5 - H_6)}{H_{supply} - H_{return}} \ \left[\frac{kg}{s}\right] \quad (30b)$$

When all essential parameters are known for each stage of the heat pump, it is possible to calculate the performance of the system. The generated heat from the subcooler and condenser is exchanged into the DH-network, and is expressed by Eq. 31:

$$Q_{out} = \dot{m}_{tot} * \left((H_4 - H_5) + (H_5 - H_6)\right) \ [W] \quad (31)$$

While the compressor work is given by following equations 32a and 32 b:

$$W_c = \dot{m} * (H_{in} - H_{out}) \ [W] \quad (32a)$$

$$W_{c,tot} = \frac{W_{c,1} + W_{c,2}}{\eta_{mech} + \eta_{elec}} \ [W] \quad (32b)$$

The system efficiency is a good indication of the heat pump performance, and it is defined as the ratio between the actual COP-value (COP) and the highest theoretical COP-value (COP_{carnot}) as in Eq. 33. The system efficiency is also used when the intermediate pressure is optimized for the specific heat demand.

$$\eta_{HP,sys} = \frac{COP}{COP_{carnot}} \quad (33)$$

Lastly, the actual COP of the heat pump and the highest theoretical COP is further expressed by equation 34a and 34b.

$$COP = \frac{Q_{out}}{W_{c,tot}} \quad (34a)$$

$$COP_{carnot} = \frac{T_{cond}}{T_{cond} - T_{evap}} \quad (34b)$$

4.4.1. Heat pump model validation

The heat pump model is validated against the results from Hu et al. (2017), further denoted as reference model. The COP-values from the reference model are significantly larger compared to the heat pump model for this study. The largest difference appears for higher waste heat temperatures, as the COP-values diverge with 27 %. The assumptions used in the reference study were not all transparently presented, which is considered a cause for the discrepancy. However, the COP-values for the reference model and the developed heat pump model both follow the same trend line as seen in Figure 17. Nevertheless, this will affect the resulting performance of the modeled heat pump negatively and thus the economical evaluation of the generated heat. Since the calculated COP-value is a most conservative approach, it was decided to proceed with the obtained model. In any case, the impact of the COP on the economics will be assessed with a sensitivity analysis.

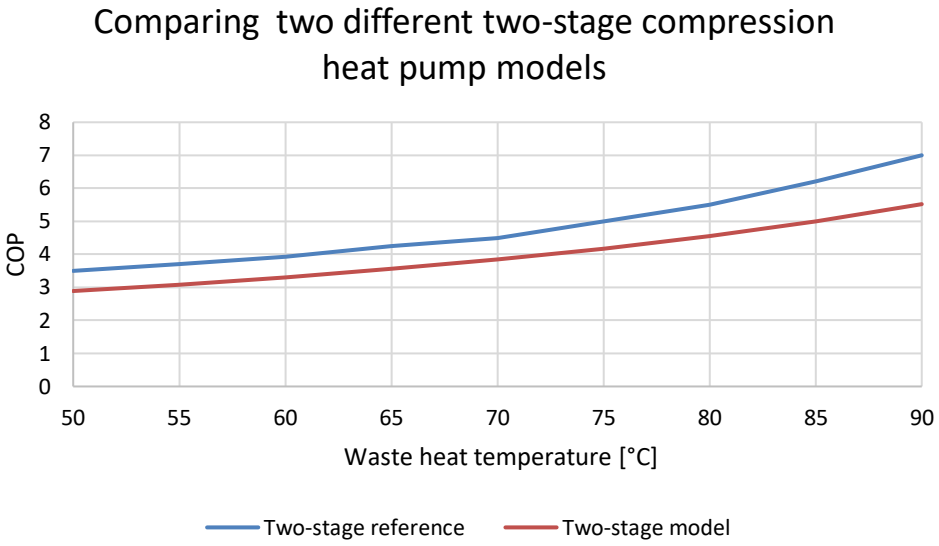

Figure 17. Graph showing the difference in the two heat pump models, where COP is a function of waste heat temperature.

4.4.2. Heat pump optimization

The heat pump must operate within the required temperatures in the district heating network. However, certain temperature intervals are more frequent than others. The frequency data of occurring temperatures over a year is compiled into different intervals, although, these are not allowed to be presented due to confidentiality. Nevertheless, the heat pump is optimized for the highest temperature occurrence rate. From an economical point of view, it is therefore relevant to optimize the heat pump for a temperature interval of 80-85 °C. The heat pump will not be in use when the DH supply temperature is below 80 °C, which also implies that the heat pump only will be in use during 48.5 % of the year.

Furthermore, the heat pump model was tested for different temperature lift intervals and intermediate pressures. The DH return temperature was fixed at a static 50 °C, while the DH supply temperature was set at intervals of 80-120 °C. The intermediate pressure is constrained between the pressure at the supply and return side. The resulting COP-values for different testing scenarios can be seen in Table 8, where the ideal intermediate pressures are highlighted in green for the corresponding temperature. The highest COP-values occur for an intermediate pressure of 7.02 bar, as can be seen in Table 8, which is why this value is optimal for the heat pump model. Thermodynamically, it is reasonable that higher COP values are achieved for smaller temperature differences. However, for each temperature, the ideal COP is observed at a different intermediate pressure. Therefore, it is important to optimize the system for the range of temperature of interest.

Table 8. Resulting COP values that are dependent on the intermediate pressure and district heating temperature (optimal values highlighted in green).

	T = 115	**T = 110**	**T = 105**	**T = 100**	**T = 95**	**T = 90**	**T = 85**	**T = 80**
Intermediate pressure [BAR]	COP	COP	COP	COP	COP	COP	COP	COP
7.02	4.73	5.28	5.94	6.77	7.84	9.28	11.35	14.55
7.66	4.78	5.32	5.98	6.79	7.83	9.22	11.19	14.20
8.30	4.82	5.35	5.99	6.77	7.78	9.10	10.96	13.75
8.94	4.84	5.35	5.97	6.73	7.69	8.95	10.68	13.24
9.57	4.84	5.34	5.93	6.66	7.57	8.75	10.36	12.69

4.5. Heat exchanger design

The supply side temperature in the DH-network is lower than the waste heat temperature throughout 50 % of the year, according to the analyzed temperature data. During this time, it is thus feasible to simply exchange the heat without the need of a heat pump. A heat exchanger is therefore added to system. When the heat exchanger is in use, the waste heat by-passes the heat pump and vice versa. Figure 18 illustrates the final schematic of the proposed system; a heat pump and heat exchanger connected to the cooling circuit and DH-network.

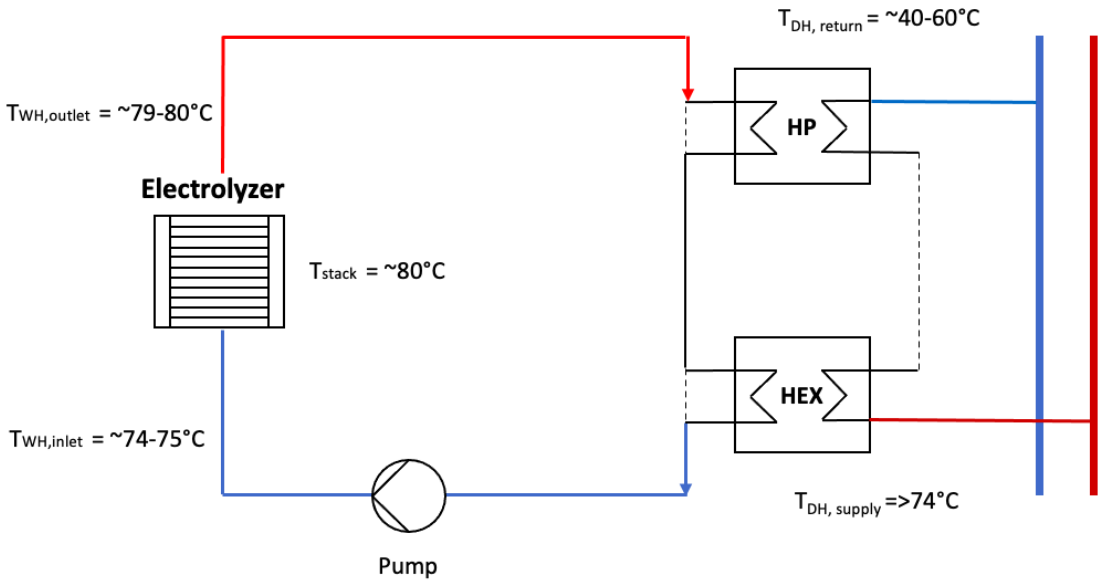

Figure 18. System schematic with heat pump and heat exchanger.

A challenge with the added heat exchanger in the cooling circuit is that the inlet and outlet temperatures of the electrolyzer must be preserved at static conditions, where the T_{out} = 79-80°C and T_{in} = 74-75 °C, whilst the DH supply and return side temperatures are vary over time. The heat pump increases the temperature of the heat source, which means that the evaporator can be designed for a suitable temperature range for the cooling circuit while still maintaining a desirable temperature output to the DH network. A heat exchanger on the other hand exchanges heat from the cooling circuit to the DH-network, which means that the unit can only be designed for a specific heat or temperature exchange. The area of the heat exchanger is static, but the mass flow of the cooling fluid can however be dynamically regulated. A by-pass valve for the heat exchanger is therefore introduced to control the inlet electrolyzer temperature and maintain it at 74-75 °C. A close-up of the heat exchanger schematic with an added by-pass valve and mixer can be seen in Figure 19.

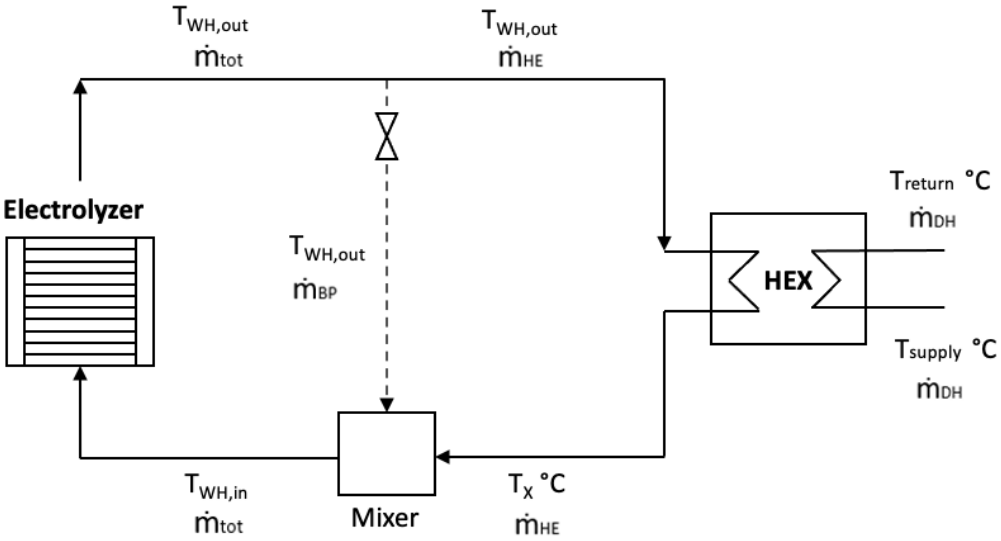

Figure 19. Heat exchanger schematic with by-pass valve.

The heat exchanger is designed with the LMTD-method. The logarithmic temperature difference (ΔT_{lm}) is calculated for the highest DH supply temperatures and lowest return temperatures i.e., during the most extreme hours. The heat exchanger is dimensioned by using Equation 35, and the assumed U-value is 2000 kW/m². In this way, the temperature after the heat exchanger (T_x) never exceeds 74 and 75 °C for the PEM and alkaline electrolyzer respectively, when 100 % of the mass flow is transferred through the heat exchanger. The outlet temperature from the mixer can therefore be controlled by varying the by-passed mass flow.

$$UA = \frac{Q_{cool}}{\Delta T_{lm}} \tag{35}$$

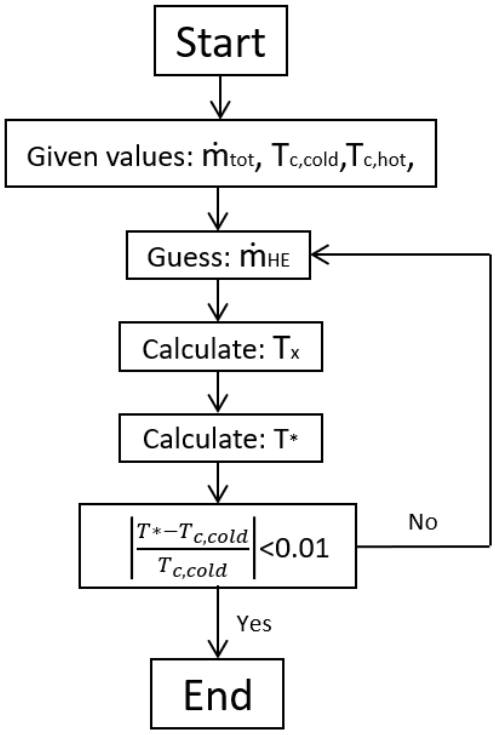

Figure 20. Flowchart of heat exchanger model.

Figure 20 shows the iterative process of calculating the actual inlet temperature of the electrolyzer. A temperature of 74-75 °C should ideally be used to cool the electrolyzer, however, a certain tolerance in the temperature span is adopted. The actual inlet temperature (T*) is therefore within 1 % of the goal temperature, which will not affect the operational conditions of the electrolyzer by a large margin. The actual inlet temperature was calculated by first introducing a factor (X) for the percentage of mass flow that goes through the heat exchanger. A constraint was added in the beginning of the iteration to avoid unreasonable values. The enthalpy after the heat exchanger, H_x, is calculated according to Eq. 36.

$$H_x = H_{co} - \left(\dot{m}_{dh} * \frac{H_{supply} - H_{return}}{\dot{m}_{cool} * X}\right) \quad (36)$$

Since the logarithmic temperature difference was initially applied for the highest DH temperature interval, a new T_{lm} was calculated from the updated values, as shown in Eq. 37 and 38.

$$dT2 = T_x - T_{return} \quad (37)$$

$$\Delta T_{lm} = \frac{dT1 - dT2}{\log\left(\frac{dT1}{dT2}\right)} \quad (38)$$

The enthalpy after the heat exchanger could then be updated before calculating the actual inlet temperature of the electrolyzer, by using equation 39.

$$H_x = H_{co} - \frac{UA * \Delta T_{lm}}{\dot{m}_{cool} * X} \quad (39)$$

Finally, the actual inlet temperature for the electrolyzer (T*) could be calculated by using an energy balance for the mixer, as in Eq. 40:

$$T* = \frac{(\dot{m}_{cool} * X * T_x) + (\dot{m}_{cool} * (1 - X) * T_{co})}{\dot{m}_{cool}} \quad (40)$$

4.5.1. Limitations of the heat exchanger system

One limitation with the heat exchanger model is that it cannot operate during conditions when the DH temperature interval (i.e. the difference between the supply and demand temperature) is too large. These extreme intervals occur sporadically during the year, which makes it difficult to dimension the heat exchanger for these conditions. These circumstances account for 55 hours per year for the PEM electrolyzer and 94 hours per year for the alkaline electrolyzer. The flexibility issues with the heat exchanger can be avoided if a thermal storage is included, since it could provide greater flexibility in the overall system. However, this implementation is outside the scope of this study and is only suggested for future work.

4.6. Dimensioning the electrical pump

The electrical pump used to circulate the water must be dimensioned in order to properly calculate an approximate electrical consumption. This consumption is often assumed to be negligible in comparison to power consumption of larger systems, as the heat pump in this case study. However, it was decided to consider the costs for the electrical pump to receive a better estimation of the LCOH. The required power for a centrifugal pump in equation 41 is defined by the pump power (P) in kW, flowrate (Q) in m³/, pump heat (H) in meters of fluid and the pump efficiency (η).

$$P = \frac{Q\rho gH}{3.6*10^6\eta} \tag{41}$$

According to Moran (2016) an efficiency of 0.7 can be used. The pump head was estimated from a pump curve - which plots the relationship between the head and required flow rate for a centrifugal pump. The actual required flow rate is higher than 80 m³/h. For a cooling circuit with a PEM electrolyzer, it was therefore assumed that 52 units are needed to cover the total flow rate of 4090 m³/h. As for a cooling circuit with an alkaline electrolyzer, approximately 79 units are needed to cover a flow rate of 6256 m³/h. Since the power consumption of the pump is of main interest, this assumption was made due to simplicity. In reality it is expected that the operation can be proceeded by, preferably, fewer pump units.

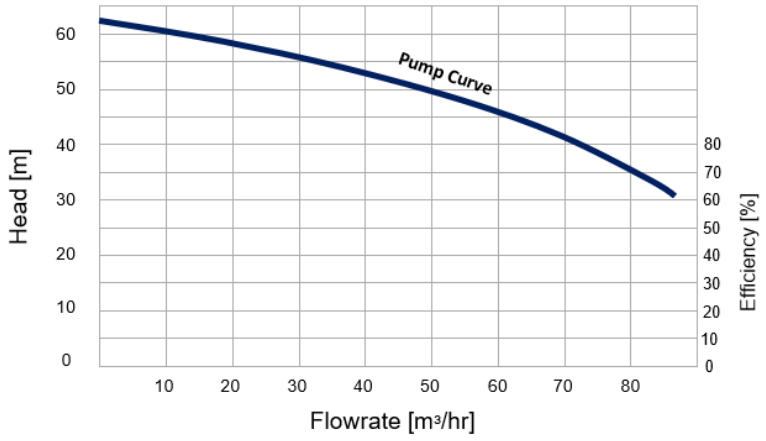

Figure 21. Pump curve with flow rate on the x-axis and pump head on the y-axis. Inspiration for illustration received from Moran (2016).

4.7. System efficiency

The electrical efficiency (η_{el}) in Equation 42 is defined as the conversion of electrical to chemical energy and more specifically the ratio between the thermoneutral voltage (V_{tn}) and cell voltage (V_{cell}). Energy is conserved according to the first law of thermodynamics - thus the electrolyzer converts electrical energy into chemical energy, where some losses are converted into heat. The thermoneutral voltage is 1.48 V at standard conditions (Shiva Kumar & Himabindu, 2019).

$$\eta_{el} = \frac{V_{tn}}{V_{cell}} \tag{42}$$

A heat to power ratio is introduced to measure the ratio of useful heat from the total electrical output:

$$ratio = \frac{Q_{useful}}{P_{tot}} \tag{43}$$

The total system efficiency (η_{tot}) is calculated by Equation 44; defined by the total heat transfer from the system to the DH-network ($Q_{out,sys}$), total required electricity for hydrogen production (W_{H2}), electricity requirement for the electrical pump (W_{pump}), heat loss from the electrolyzer stack (Q_{loss}) and electricity input to the total system (W_{in}).

$$\eta_{tot} = \frac{Q_{out,sys} + W_{H2} - Q_{loss,electro}}{W_{in} + W_{pump}} \tag{44}$$

4.8. Levelized cost of heat

Levelized cost of heat (LCOH) is calculated to determine the cost effectiveness of the generated heat from the system. The LCOH approach is considering the initial investment costs of components, operational and maintenance costs, and generated energy over the lifetime of the system. The equation is given by:

$$LCOE = \frac{\sum_{t=0}^{n} \frac{I_t + M_t}{(1+r)^t}}{\sum_{t=0}^{n} \frac{E_t}{(1+r)^t}} \tag{45}$$

where I_t is the CAPEX, M_t is the OPEX including electricity costs, E_t is the is the thermal energy generation, r is the discount rate and n is the lifetime of the system in year t. Year t = 0 refers to the start-up of the system. A discount rate of 10 % and a lifespan of 20 years was considered in the calculations, as well as a 2 % inflation rate.

Three main components of the system were considered for the CAPEX calculations of the system, i.e. large-scale heat pump, heat exchanger and an electrical pump required for circulating the water throughout the circuit. The OPEX is including day-to-day operational management costs and electrical costs for compressors in the heat pump and electrical pump. The operational costs are assumed to be 2 % of the total CAPEX, while the electrical costs are calculated from the actual power consumption. The electricity price is calculated by the average monthly spot prices for the SE1 power-domain in Sweden, during the years 2018-2021. CAPEX

and OPEX estimations can be seen in Table 9 for a system with PEM electrolyzer, and Table 10 for a system with alkaline electrolyzer. The average electricity prices are available in Table 11.

Table 9. CAPEX and OPEX for system with PEM electrolyzer.

CAPEX			**Source**
Heat pump	5500	SEK/kW_{th}	Internal industrial partner (2022)
Heat pump	161 425 000	SEK/unit	
Centrifugal pump	475 000	SEK/req. power	Shamoushaki et al. (2021). *Centrifugal*
Heat exchanger	22 420 000	SEK/req. area	Shamoushaki et al. (2021). *Flat plate*
Total CAPEX	184 320 000	SEK	
OPEX			
Electrical costs: heat pump	9 676 000	SEK/year	
Electrical costs: centrifugal pump	416 000	SEK/year	
Operational management, 2% of CAPEX	3 686 000	SEK/year	
Total OPEX	13 778 000	SEK/year	

Table 10. CAPEX and OPEX for system with alkaline electrolyzer.

CAPEX			**Source**
Heat pump	5000	SEK/kW_{th}	Internal industrial partner (2022)
Heat pump	223 600 000	SEK/unit	
Centrifugal pump	618 000	SEK/req.power	Shamoushaki et al. (2021). *Centrifugal*
Heat exchanger	31 949 000	SEK/req. area	Shamoushaki et al. (2021). *Flat plate*
Total CAPEX	256 167 000	SEK	
OPEX			
Electrical costs: heat pump	13 613 000	SEK/year	
Electrical costs: centrifugal pump	636 000	SEK/year	
Operational management, 2% of CAPEX	5 571 000	SEK/year	
Total OPEX	19 820 000	SEK/year	

The electricity price usually consists of three components: spot price, energy tax and an electricity network fee. Luleå Energy is the owner of the electrical grid in Luleå, as to why it can be assumed that the network fee can be neglected. Hence, the electricity price is considered to have two components only in this case study which is the spot price and energy tax. The spot price is varying day-by-day, which is why it can be favourable to use an average price setting. The energy tax for 2022 is 0.45 SEK/kWh with a tax-fee of 25 % included, according to Ellevio (2022).

Table 11. Spot prices retrieved from Elpriser24 (n.d.)

Monthly average electricity prices including energy tax [SEK/kWh$_e$]	
January	0.84
February	0.814
Mars	0.76
April	0.74
May	0.75
June	0.74
July	0.83
August	0.88
September	0.89
October	0.78
November	0.81
December	0.88

5. RESULTS

The results will be divided into several parts. First, the technical details of the system will be presented which are divided into electrolyzer thermal output, heat transfer to the DH-network, and the total system performance. Finally, LCOH and sensitivity analyses are presented.

5.1. Electrolyzer thermal output

Operating temperatures, thermal power output, and extracted heat from the PEM and alkaline electrolyzers are presented in this chapter.

5.1.1. PEM electrolyzer

Figure 22a illustrates the thermal power output from the electrolyzer stack (left axis) and the fraction of useful excess heat (right axis) as a function of cell temperature and current density. The graph shows that the thermal output is dependent on the operational conditions of the electrolyzer, where lower operational temperatures offer a higher output. However, that also accounts for larger electrical losses which is unfavorable for hydrogen production.

Figure 22b shows the waste heat temperature from the electrolyzer stack. Higher current densities result in increased losses, which causes the outlet temperature to deviate from the cell temperature. The purpose of presenting the graphs in Figure 22a and 22b is to show how different operational conditions can affect the performance of the electrolyzer stack.

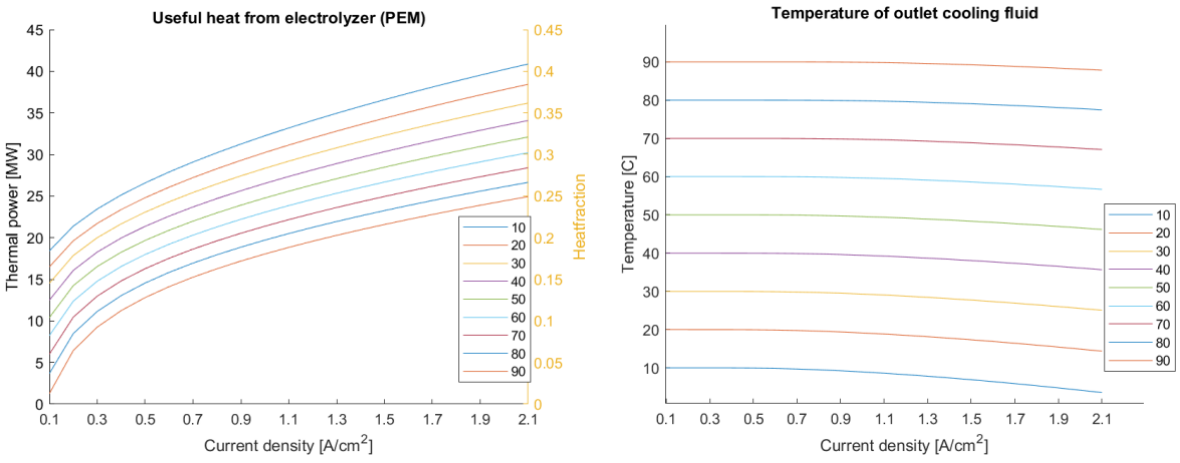

a) *b)*

Figure 22. PEM: Thermal power output and fraction of usable waste heat, as a function of current density and temperature (a). Outlet temperature of the PEM electrolyzer, as a function of current density (b).

The results of the electrochemical and thermal modelling of the PEM electrolyzer are presented in Table 12. The annual extracted heat from the stack is 203 060 MWh_{th}. In this study, the PEM electrolyzer is chosen to have a current density of 1.5 A/cm² and a cell temperature of 80 °C.

Table 12. Electrochemical and thermal results from the PEM electrolyzer model.

Parameters	Value
Required number of cells	34 530
Cell voltage [V]	1.93
Current density [A/cm²]	1.5
Cell temperature [°C]	80
Waste heat temperature [°C]	79
Cooling fluid temperature [°C]	74
Hydrogen production [kg/hour]	1929
Electrical efficiency [%]	76.7
Mass flow of cooling fluid [kg/s]	1108
Heat/Electric power ratio	0.23
Waste heat output from stack [MW_{th}]	23.2
Extracted waste heat from stack [%]	23.2
Extracted heat from the stack [MW_{th}/yr]	203 060

5.1.2. Alkaline electrolyzer

Figure 23a shows the thermal power output from the electrolyzer stack (left axis) and the fraction of useful excess heat (right axis) as a function of cell temperature and current density. The excess heat is higher for the alkaline electrolyzer, than for the PEM counterpart.

Figure 23b illustrates the temperature of the waste heat from the electrolyzer stack. The graph presents straighter lines in comparison to Figure 22b, meaning that the temperature of the cooling fluid is very close to the alkaline cell temperature.

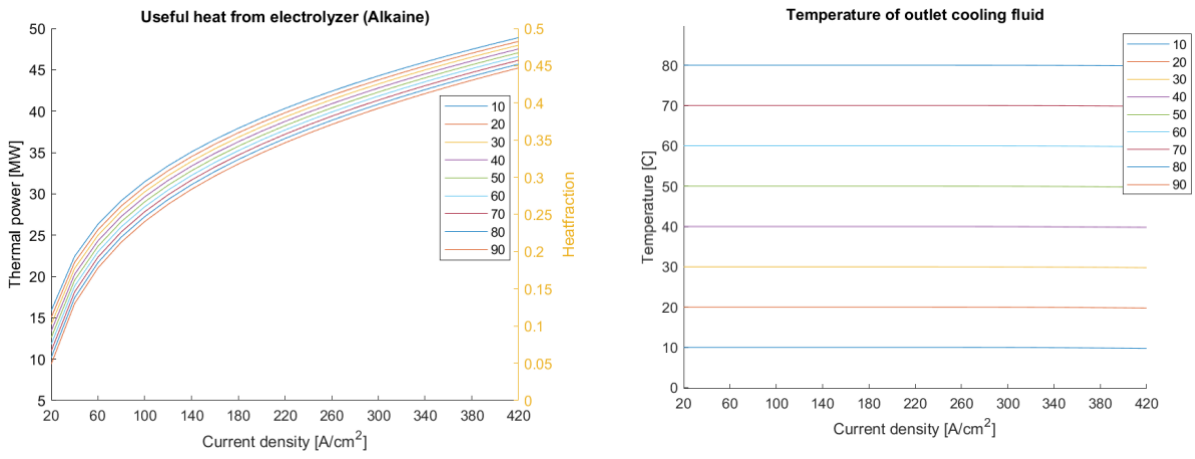

a) *b)*

Figure 23. Alkaline: Thermal power output and fraction of usable waste heat, as a function of current density and temperature (a). Outlet temperature of the alkaline electrolyzer, as a function of current density (b).

Table 13 presents the results of the electrochemical and thermal modelling of the alkaline electrolyzer. In this study, the alkaline electrolyzer is chosen to have a current of 200 Amperes and an 80 °C cell temperature.

Table 13. Electrochemical and thermal results from the alkaline electrolyzer model.

Parameters	Value
Required number of cells	218 030
Cell voltage [V]	2.29
Current [A]	200
Cell temperature [°C]	80
Waste heat temperature [°C]	80
Cooling fluid temperature [°C]	75
Hydrogen production [kg/hour]	1624
Electrical efficiency [%]	64.5
Mass flow of cooling fluid [kg/s]	1694
Heat/Electric power ratio	0.35
Waste heat output from stack [MW_{th}]	35.5
Extracted waste heat from stack [%]	35.5
Extracted heat from the stack [MWh_{th}/yr]	310 630

5.2. Recovered heat for the DH-network

Results for the waste heat transfer to the DH-network are presented in this chapter.

5.2.1. PEM electrolyzer system

Figure 24a presents the results of the modelled waste heat transfer from a heat pump to the DH-network. The heat pump is operating during hours when the DH supply temperature is lower than the waste heat temperature (i.e. >79 ◦C), which occurs during periods of lower outdoor temperatures. In Luleå, colder outdoor temperatures mainly occur during late fall, winter and early spring. In contrast, the heat exchanger is utilized during hours when the waste heat temperature is higher than the DH supply temperature (i.e. <79 ◦C), which primarily occurs during the warmer periods of the year. Warmer outdoor temperatures are present during late spring, summer and early fall. The waste heat transfer from the heat exchanger to the DH-network is presented in Figure 24b.

The thermal output from the heat pump is significantly larger than for the heat exchanger. This is because the DH supply demand is higher during low outdoor temperatures. During high outdoor temperatures, the DH supply temperature decreases. Thus, it is sufficient to utilize a heat exchanger that allows for lower thermal outputs. However, the heat exchanger is not able to transfer all available waste heat into the DH-network due to dimensioning constraints of the unit.

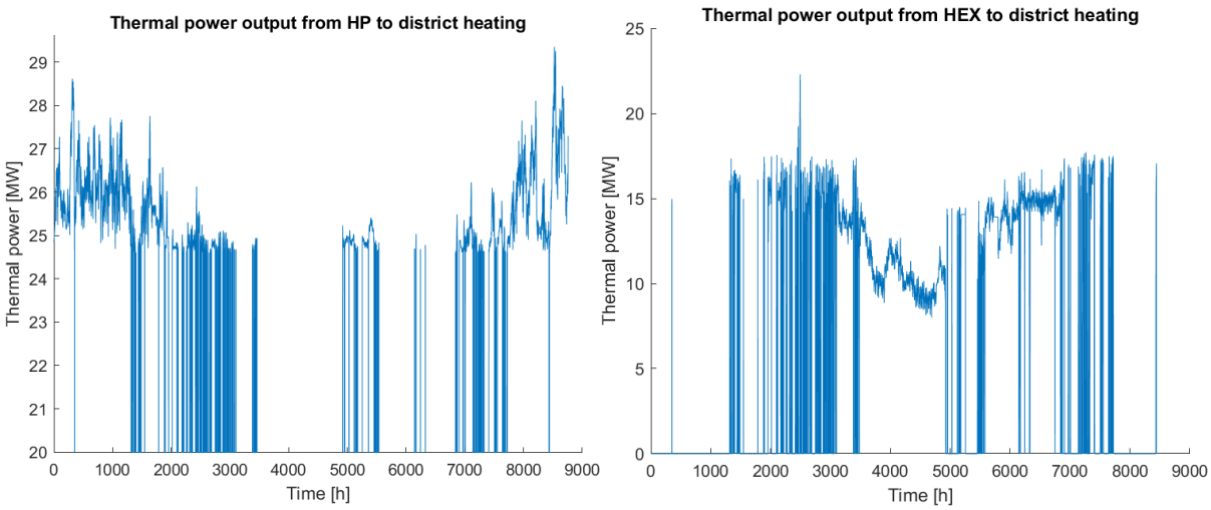

a) *b)*

Figure 24. PEM: Thermal power output from the heat pump to the DH-network over a year (a). Thermal power output from heat exchanger to the DH-network over a year (b).

Figure 26a shows the COP value of the heat pump. The heat pump has a higher efficiency during spring and autumn, where it reaches a COP-value of ~16, whilst lower values occur during winter hours. The variation in efficiency is related to the required temperature lift – low temperature lifts results in a higher efficiency, while high temperature lifts decreases the efficiency of the heat pump.

Figure 26b illustrates the inlet temperature of the cooling fluid entering the PEM electrolyzer stack. Ideally, the entering temperature should be static at 74 °C to maintain the cell temperature at 80 °C. In reality, the temperature however ranges from 73.4 to 74.7 °C. This occurs when the heat exchanger is utilized, as static dimension of the heat exchanger design does not allow for a dynamic control of the cooling fluid temperature. Nevertheless, the temperature is maintained within an acceptable variance due to the by-pass valve introduced in section 4.5.

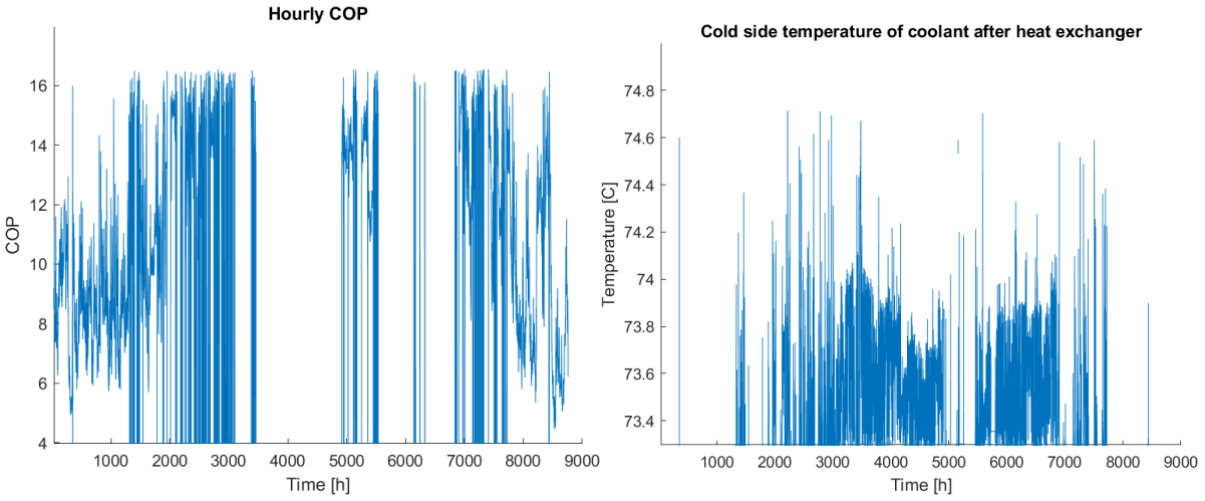

a) *b)*

Figure 25. PEM: Heat pump COP value as a function of time (a). Temperature of the cold side of coolant during heat exchanger usage (b).

As previously mentioned, the heat pump is utilized when the supply temperatures in the DH-network are above 79 °C. The thermal annual output from the heat pump to the DH-network is presented in Table 14. The required peak thermal power for the heat pump is 29.35 MW_{th}, which results in an average COP value of 10.

Table 14. PEM: Heat pump parameters.

HP parameter	Value
Thermal waste heat input to HP [MWh_{th}/year]	105 690
Compressor electricity requirement [MWh_e/yr]	11 760
Heat pump output to DH [MWh_{th}/year]	116 630
Peak thermal power [MW_{th}]	29.35
Maximum COP	16.5
Average COP	9.9
Annual operation ratio [%]	52

The heat exchanger is utilized when the DH supply temperatures are below 79 °C. The thermal annual output to the DH-network is 53 percent less through the heat exchanger compared to the heat pump, which can be seen in Table 15. To manage flexibility for different DH supply temperatures, the heat exchanger is dimensioned for an optimal static UA-value, also presented in Table 15. However, the UA-value cannot be dimensioned for all supply temperatures. Due to this and the static dimension of the heat exchanger, one occurring constraint is that it cannot cope with certain conditions in the DH-network during about 50 hours over the course of one year, as previously discussed.

Table 15. PEM: Heat exchanger parameters.

HE parameter	Value
Thermal heat output to DH [MWh_{th}/year]	55 140
Average waste heat power output [MW_{th}]	13.1
UA [kW/K]	3969
Annual operation ratio [%]	48
Operational constraint of heat exchanger [h]	50

5.2.2. Alkaline electrolyzer system

Figure 27a shows the results of the modelled waste heat transfer from the heat pump to the DH-network. The heat pump operates during the hours when the DH supply temperature is higher than the waste heat temperature (i.e. >80 ◦C), which occurs during low outdoor temperatures. In contrast, the heat transfer from the heat exchanger to the DH-network (illustrated in Figure 27b) is utilized during hours when the waste heat temperature is higher than the DH supply temperature (i.e. <80 ◦C). In general, the results are similar as for the PEM electrolyzer system. Although, the thermal power output from the heat pump is significantly larger as compared to the PEM system, since the available waste heat from the alkaline electrolyzer is higher.

For the heat exchanger, the thermal heat transfer is similar as for the PEM system, even though the alkaline electrolyzer yields higher waste heat losses. This is because the DH supply demand is equal for both systems. The mass flow in the DH network would need to be increased from the normal operating conditions to provide for a higher thermal output from the heat exchanger.

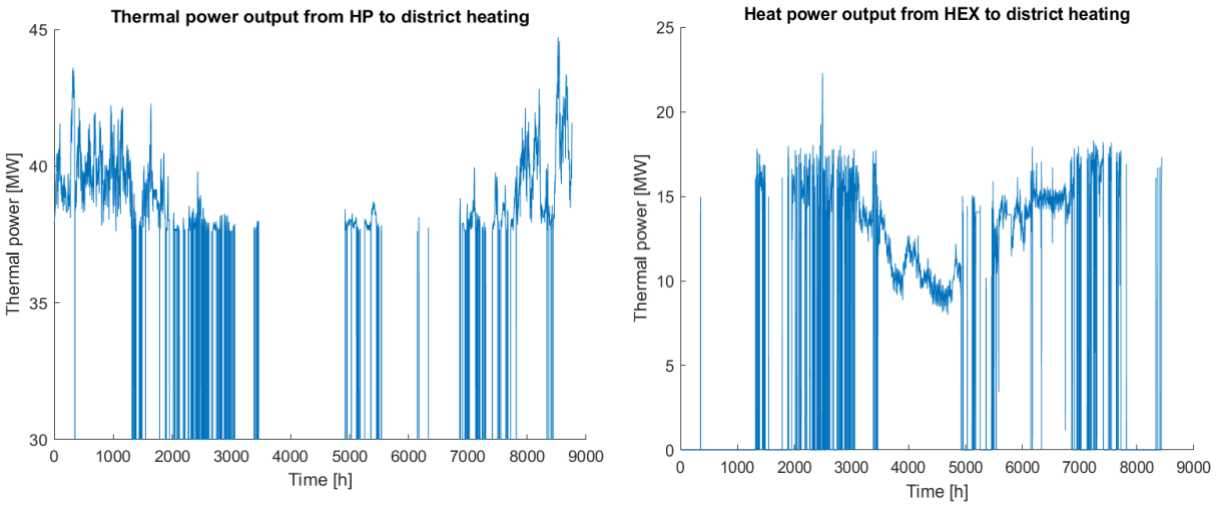

a) *b)*

Figure 26. Alkaline: Thermal power output from the heat pump to the DH-network over a year (a). Thermal power output from heat exchanger to the DH-network over a year (b).

Variations in COP-values of the heat pump throughout one year is illustrated in Figure 29a. Modelling results shows that the peak COP-values are slightly higher than for a heat pump connected to the PEM electrolyzer i.e., by ~1 %. This is because the waste heat temperature from the alkaline electrolyzer is higher than for PEM, which lowers the temperature upgrading interval and increases the efficiency. Figure 29b shows the temperature of the cooling fluid that enters the alkaline electrolyzer. Ideally, the temperature should be maintained at 75 °C, however, the temperature variance of 1.2 °C is within acceptable limits to preserve the desirable cell temperature of 80 °C.

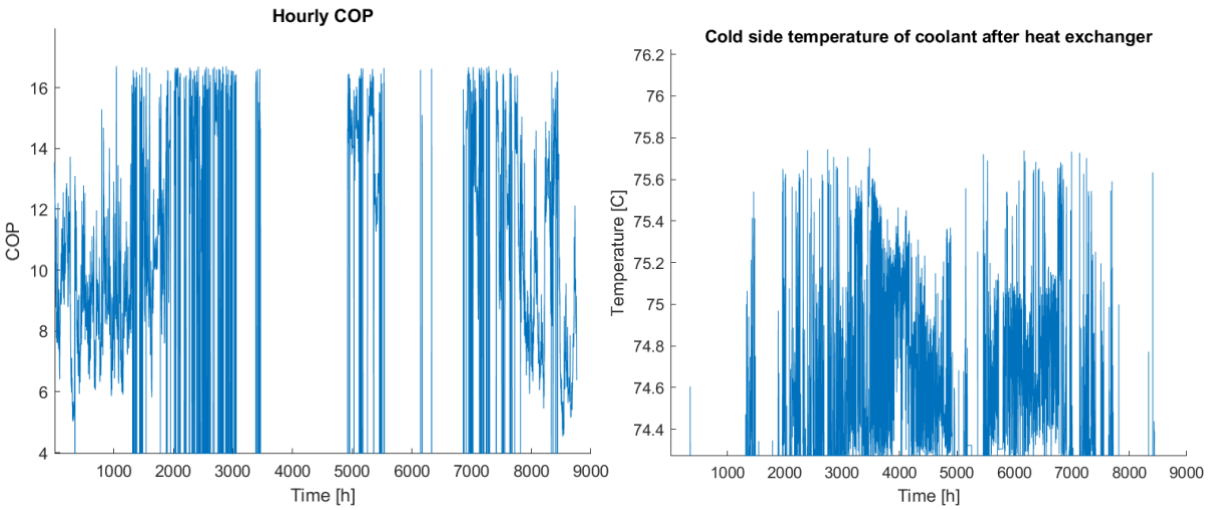

a) *b)*

Figure 27. Alkaline: Hourly COP values over the year (a). Hourly cold side temperature of coolant into the electrolyzer (b).

The thermal heat pump output to the DH is presented in Table 16 below. The thermal output is significantly higher in comparison to the PEM system. The reason is because the alkaline electrolyzer provides a higher thermal loss, which requires an increased mass flow of the cooling fluid. Thus, a higher amount of thermal heat can be transferred to the heat pump and heat exchanger. The peak thermal power is also higher in comparison to the PEM connected heat pump, i.e. by ~15 MW_{th}, which requires a larger heat pump.

Table 16. Alkaline: Heat pump parameters.

HP parameter	Value
Thermal waste heat input to HP [MWh_{th}/year]	151 090
Compressor electricity requirement [MWh_e/yr]	16 510
Heat pump output to DH [MWh_{th}/year]	166 470
Peak thermal power [MW_{th}]	44.7
Maximum COP	16.7
Average COP	10.1
Annual operation ratio [%]	48.5

The thermal heat output to the DH from the heat exchanger is presented in Table 17. The area of the heat exchanger is increased significantly in comparison to the PEM connected heat exchanger. This stems from the increased utilization of the heat exchanger throughout the year, which lead to increased temperature intervals for the waste heat and DH supply temperature. Thus, it requires an increased heat exchanger area. Probably, the reason for this is because the amount of DH temperatures that are within critical regions are increased (i.e. temperature regions for which the static dimension of the heat exchanger cannot operate for).

Table 17. Alkaline: Heat exchanger parameters.

HE parameter	Value
Thermal heat output to DH [MWh_{th}/year]	59 750
Average waste heat power output [MW_{th}]	13.3
UA [kW/K]	5701
Annual operation ratio [%]	51.5
Operational constraint of heat exchanger [h]	76

5.3. System performance

In this chapter, the system efficiency and total thermal heat output to the DH-network are presented for both PEM and alkaline connected systems.

5.3.1. PEM electrolyzer system

The overall efficiency of the system increases from 76.66 % to 94.7 % when waste heat recovery is implemented i.e., a heat pump and heat exchanger are installed. System losses account for approximately 5.3 %, where most of it is because the heat exchanger is not able to utilize all available waste heat. The performance of the overall system is presented in Table 18 where the electricity to hydrogen efficiency is calculated by Equation 42, while the system efficiency is given by Equation 44. Furthermore, it is possible to extract 203 060 MWh/year of thermal energy from the PEM electrolyzer stack. However, 171 770 MWh/year could be implemented onto the DH network due to losses, mainly in the HEX system.

Table 18. PEM: Results of the overall system outputs.

PEM	
Total parameter	**Value**
Extracted heat from stack [MWh_{th}/year]	203 060
Heat losses from electrolyzer [MWh_{th}/year]	1420
Total output to DH [MWh_{th}/year]	171 770
Average waste heat output to DH [MW_{th}]	19.6
Electricity input to electrolyzer [MWh_e/year]	876 000
Electricity used for hydrogen conversion [MWh_e/year]	671 540
Compressor electricity requirement for HP [MWh_e/year]	11 760
Pump electricity usage [MWh_e/year]	522
Electricity to hydrogen efficiency [%]	76.66
Overall system efficiency [%]	94.7

5.3.2. Alkaline electrolyzer system

The overall system performance for an alkaline connected electrolyzer is presented in Table 19. The total overall efficiency of the system increases from 64.54 % to 88.39 % when a waste heat recovery system is implemented. The alkaline system is less efficient than the PEM counterpart, mainly because the heat exchanger is not able to utilize all available waste heat. Similarly, to the PEM system, the alkaline system has losses in the HEX system which results in a total output to the DH network of 226 220 MWh_{th}/year of the originally extracted 310 630 MWh_{th}/year.

Table 19. Alkaline: Results of the overall system outputs.

Alkaline	
Total parameter	**Value**
Extracted heat from stack [MWh_{th}/year]	310 630
Heat losses from electrolyzer stack [MWh_{th}/year]	3.14
Total output to DH [MWh_{th}/year]	226 220
Average waste heat output to DH [MW_{th}]	25.8
Electricity input to electrolyzer [MWh_e/year]	876 000
Electricity used for hydrogen conversion [MWh_e/year]	565 370
Compressor electricity requirement for HP [MWh_e/year]	16 510
Pump electricity usage [MWh_e/year]	793
Electricity to hydrogen efficiency [%]	64.54
Overall system efficiency [%]	88.39

5.4. Levelized cost of heat

5.4.1. PEM electrolyzer system

With the used investment costs and electricity price presented in Figure 30, the LCOH is 0.218 SEK/kWh$_{th}$ with a discount rate of 10 %. This price is not including the required added taxes of 25 %. Whether an LCOE of 0.218 SEK/kWh$_{th}$ is cost competitive depends on other available fuel alternatives for heat generation and the market prices for district heating. Possible incentives for the investment could also reduce the LCOH, making it even more profitable.

The calculated LCOH however includes uncertainties. It is a difficulty to choose the most appropriate discount rate, find trustworthy investment costs and estimate future electricity prices. Also, the heat pump validation in chapter 4.4.1 illustrates that the COP values does not correspond to the values from the reference study by Hu et al. (2017). Due to this, a sensitivity analysis for the calculated LCOH was therefore performed for variations in chosen discount rates, variations in the estimated CAPEX, electricity prices and heat pump COP values. To maintain consistency, the values were tested for an increase and decrease of 30% respectively. As can be seen in figure 30, CAPEX costs highly affect the LCOH. As for the COP values, low COP affect the LCOH more than high COP values. However, it is not the most influential factor for the LCOH calculations, which can further validate that the calculated heat pump COP-values can grant a trustworthy indication of the overall performance of the system.

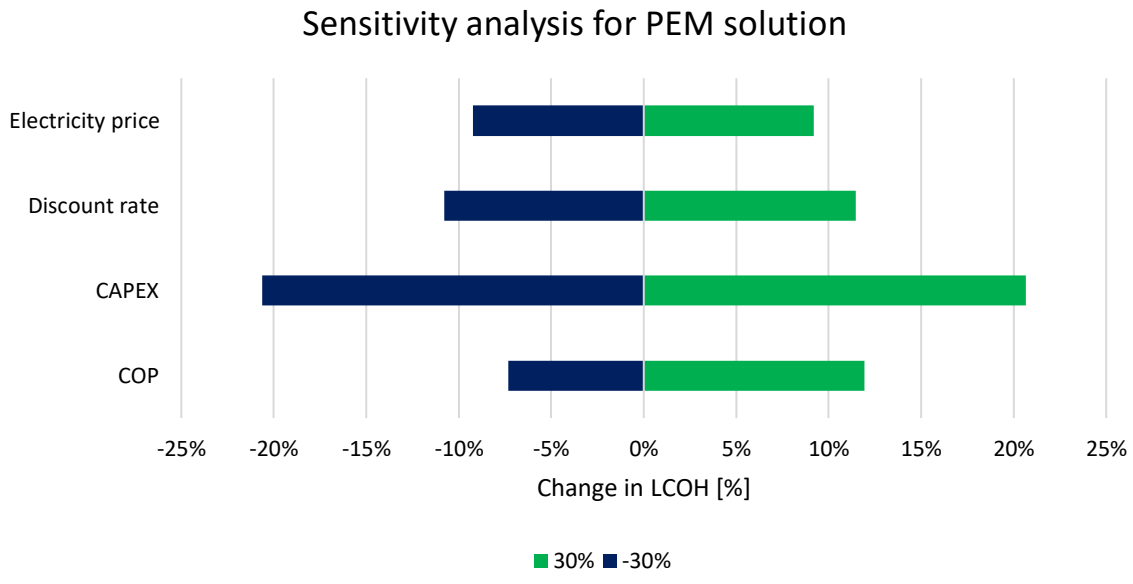

Figure 28. Sensitivity analysis: PEM.

5.4.2. Alkaline electrolyzer system

The LCOH for a system with an alkaline electrolyzer is 0.23 SEK/kWh$_{th}$. A sensitivity analysis for electricity price, discount rates, CAPEX and heat pump COP-value is illustrated in Figure 31. The percentual change in LCOH is similar as for the PEM electrolyzer system.

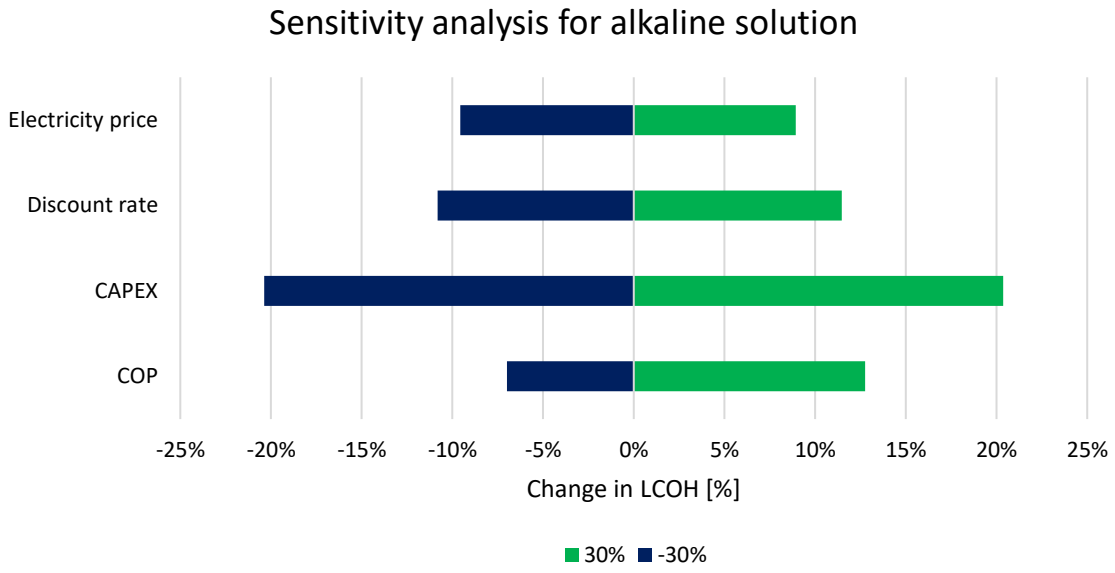

Figure 29. Sensitivity analysis: alkaline.

5.4.3. Future scenario: lower supply temperatures

Future DH networks will have lower supply temperatures. Therefore, a sensitivity analysis is performed for a future scenario with decreased supply temperatures. For a system with a PEM electrolyzer, the LCOH is 0.2 SEK/kWh$_{th}$ for a supply temperature of 92 °C, while it is 0.218 SEK/kWh$_{th}$ for a system with an alkaline electrolyzer as seen in Figure 32. This is a decrease of 7.8 % and 5.2 %. This decrease in costs relates to lower heat pump investment costs and required compression power.

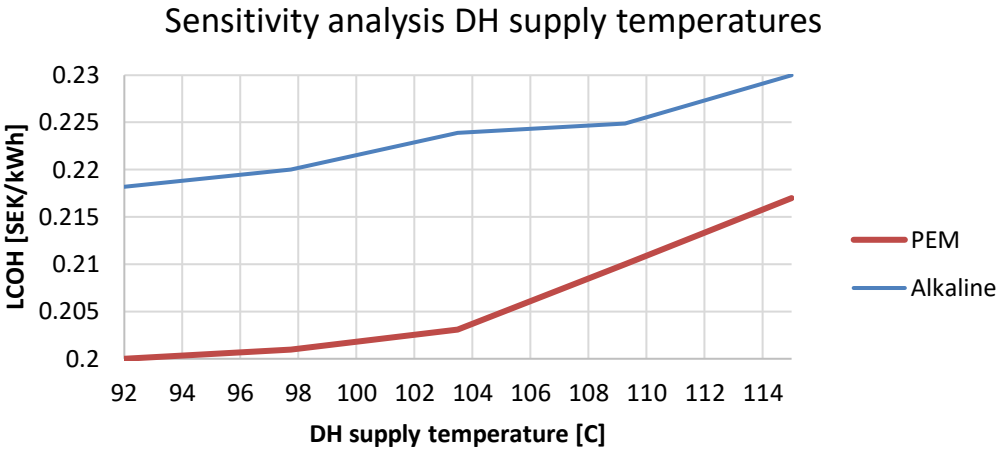

Figure 30. Sensitivity analysis for DH supply temperatures

If DH supply temperatures are below 80 °C in future DH-networks, a heat pump would not be required for waste heat utilization. Instead, only a heat exchanger would be applied. A rough approximation of the LCOH for this type of waste heat utilization system is presented in Figure 33 - where the LCOH is 0.018 SEK/kWh$_{th}$ for a PEM electrolyzer connected system, and 0.017 SEK/kWh$_{th}$ for a system with an alkaline electrolyzer.

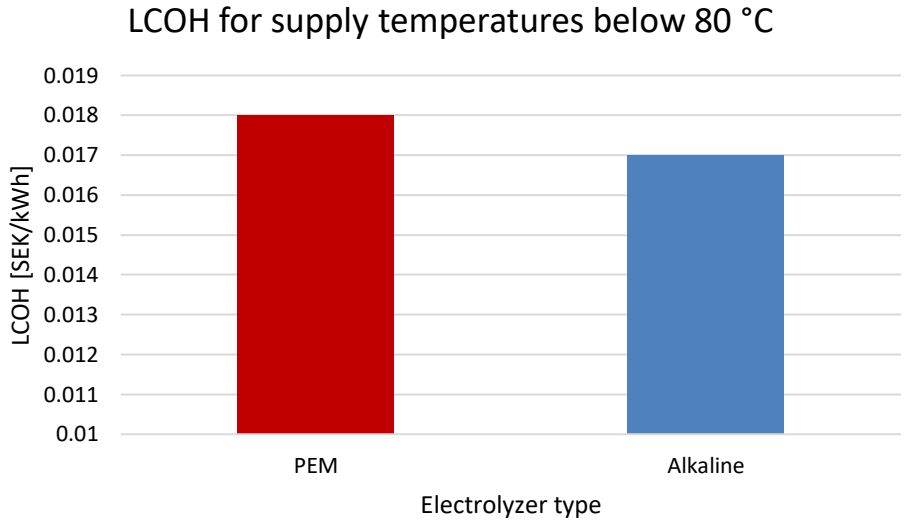

Figure 31. LCOH for supply temperatures below 80 °C.

6. DISCUSSION

The proposed system for waste heat upgradation consists of a two-unit solution, where a heat pump and heat exchanger are utilized to transfer waste heat into the DH-network. The heat pump operates when DH supply temperatures are above ~80 °C, which is mainly during fall, winter and spring periods. The opposite operational conditions apply for the heat exchanger, where it is dimensioned for operation below ~80 °C, therefore it is mainly utilized during summer months. Although, one operational constraint of the system is that heat cannot be upgraded during some hours during the year; 50 hours for a PEM connected system and 76 hours for an alkaline electrolyzer system. This is due to the un-flexible dimensioning of the heat exchanger, which is not able to cover all heat loads. However, this issue could be resolved by transferring the heat to an integrated thermal heat storage. The latter solution has not been investigated and modelled for in this case study, but it is reasonable to assume that it would offer higher operational flexibility to the proposed system and increase the overall system efficiency. Simultaneously, this would also maintain the required need of cooling for the electrolyzer stack.

One benefit of the proposed two-unit system is that it offers a simplified maintenance; service can be planned for one unit at a time to maintain the overall performance of the system. Maintenance for the heat exchanger is suitable during winter months, while it is more suitable during summer for the heat pump in order to not affect the output performance. Another advantage is that the system would allow ABB to avoid further costs associated with cooling of the electrolyzer – since cooling is offered simultaneously while extracting and utilizing the waste heat. A disadvantage with this configuration is however that it is highly dependent on the required load on the DH-network. The cooling of the electrolyzer is affected when the heat load on the DH-network is lower than the produced load from the heat pump or heat exchanger, or if maintenance work and other general issues affect the DH-operation. These disturbances would not allow the electrolyzer to produce hydrogen due to affected cooling performance. However, this is also an issue that could be resolved by an integrated thermal heat storage – which allows the electrolyzer to operate and the excess heat to be stored even if the DH-network cannot allow for integration of heat at some points during a year.

The proposed waste heat recovery system does not only provide cooling to the electrolyzer stack and heat to the DH-network, it also generates the heat to a competitive price. In comparison to the LCOH costs for different thermal energy sources presented in Table 2, the calculated LCOH costs for the generated waste heat from the electrolyzers are up to half as low.

6.1. Electricity prices

The sensitivity analysis in Figure 30 and 31 illustrates that the electricity price is one of the factors that have the least amount of impact on the LCOH. In this study, the LCOH is only calculated with regards to the generated waste heat – where the heat pump compressors and the electrical pump are affected by variations in electricity price. In reality, the electrolyzer stack is however partly fed with electricity from the grid which implies that the system in total

is dependent on variations in electricity price. It is not reasonable to produce hydrogen if the electricity price out-conquers the selling price of hydrogen and heat. Nonetheless, the waste heat offers the possibility to act as a buffer to give economic leeway – the heat can be sold for a higher price during periods of critical high electricity prices. Thus, if the whole system is considered, the sensitivity analysis of the electricity price is therefore deceptive as it may affect the LCOH more than what is shown in the figures. Another factor that could lower the LCOH, which is not mentioned previously, is if the heat pump and heat exchanger investment would be partly covered by economic incentives. It is legitimate to consider investment alleviations as the green hydrogen evolution is encouraged with endorsement by the Swedish national hydrogen strategy.

6.2. Future scenarios

As previously mentioned in the literature review, future DH-networks will have lower supply temperatures. A sensitivity analysis of the LCOH showed that supply temperatures of 92 degrees would decrease the LCOH for PEM and alkaline connected systems with 7.8 and 5.2 percent, respectively. This decrease in costs relates to a lower of heat pump investment costs and required compression power. The reason for the latter cause is due to a lower requirement of temperature lift. What is not taken into regard, however, is the type of heat pump that would be needed for lower temperature lifts. For a supply temperature of 80 degrees, it is reasonable to assume that a smaller and less complex upgrading system could be applied. For example, a heat pump with one-stage compression could be used instead of two-stage compression. Less components means lower investment and maintenance costs, which consecutively decreases the LCOH further than already calculated for in the sensitivity analysis. Due to CAPEX costs being the most influential factor for the LCOH calculations, it is therefore reasonable to assume that generated heat from the proposed system could be more price competitive if applied to a fourth generation of district heating network. As mentioned in section 5.4.3, a DH-network with low supply temperatures would perhaps not require a heat pump for waste heat upgradation – instead, a heat exchanger could be sufficient. The heat pump investment cost reaches up to ~88 % of the total CAPEX of the system, which therefore would reduce the LCOH to 0.018 and 0.017 SEK/kWh_{th} (for PEM and Alkaline based system, respectively) in a scenario where a heat pump is not required. Furthermore, if taxes on non-utilized waste heat are introduced in the future the proposed system would also provide economic benefits in terms of that.

However, it is worth to mention that the LCOH for the future scenarios are complex to estimate accurately since the model of this study is not dimensioned for lower supply temperatures and the future electricity price is not predicted. Therefore, the presented future costs should not be seen as an absolute veraciousness, but rather as a predictive trend.

7. CONCLUSIONS

How much heat can be extracted from a PEM and alkaline electrolyzer stack with an installed capacity of 100 MW?

It is possible to extract 203 060 MWh_{th} from a PEM electrolyzer stack, while 310 630 MWh_{th} can be extracted from an alkaline electrolyzer stack annually.

How much waste heat can be utilized on the DH-network in Luleå?

The results from the modelled system with a PEM connected electrolyzer suggests that 171 770 MWh_{th} can be integrated onto the DH-network annually. For a system with an alkaline connected electrolyzer, 226 220 MWh_{th} can be transferred to the DH-network annually. All available waste heat cannot be transferred to the DH-network during summer periods due to dimensioning constraints of the heat exchanger. Hence, the integrated amount of heat is lower than the extracted heat from the electrolyzer stack.

What is the performance of the overall system?

The overall efficiency of the PEM electrolyzer system is 94.7 % when the waste heat is utilized, while the overall efficiency is 88.39 % for the alkaline electrolyzer system.

What is the Levelized Cost of Heat (LCOH) of the utilized waste heat and what are the factors that affect the economic feasibility?

The calculated LCOH is 0.218 SEK/kWh_{th} for the PEM electrolyzer system, while it is 0.23 SEK/kWh_{th} for the alkaline electrolyzer system. The sensitivity analysis implies that the CAPEX factor has largest impact on the LCOH, which entails that the LCOH for the alkaline electrolyzer system is slighty higher than for the PEM electrolyzer system due to increased investment costs. However, the utilized heat is still price competitive and nearly half as low in comparison to other heat generation alternatives - such as biomass fired boiler or wood chip fuelled CHP plant. Furthermore, calculations for future scenarios predicts that the LCOH can be further decreased. DH supply temperatures below 80 ^{o}C eliminates the requirement of a heat pump, which lowers the initial investment cost for the proposed system by ~88 %. This scenario provides for a significantly lower LCOH, which implies that the proposed system of this study can offer higher profitability in the future.

8. SUGGESTIONS FOR FURTHER WORK

In this study, the proposed system was modelled for static conditions, which is a simplification of reality. To add depth to the model, it would be beneficial to model the system for dynamic conditions. Optimization modelling would also increase the flexibility of the system, as well as adding a thermal heat storage for reliability of the cooling.

Furthermore, it would also be interesting to investigate how the excess heat from hydrogen compression can be extracted. Surely, more heat could be utilized on the DH-network and perhaps the waste heat temperature would also be increased - meaning that the LCOH could be further decreased.

REFERENCES

Abdin, Z., Webb, C. J., & Gray, E. M. (2015). Modelling and simulation of a proton exchange membrane (PEM) electrolyser cell. *International Journal of Hydrogen Energy*, *40*(39), 13243–13257. https://doi.org/10.1016/J.IJHYDENE.2015.07.129

Averfalk, H., Ingvarsson, P., Persson, U., Gong, M., & Werner, S. (2017). Large heat pumps in Swedish district heating systems. *Renewable and Sustainable Energy Reviews*, *79*, 1275–1284. https://doi.org/10.1016/J.RSER.2017.05.135

Awasthi, A., Scott, K., & Basu, S. (2011). Dynamic modeling and simulation of a proton exchange membrane electrolyzer for hydrogen production. *International Journal of Hydrogen Energy*, *36*(22), 14779–14786. https://doi.org/10.1016/J.IJHYDENE.2011.03.045

Ball, M., & Wietschel, M. (2009). The future of hydrogen – opportunities and challenges. *International Journal of Hydrogen Energy*, *34*(2), 615–627. https://doi.org/10.1016/J.IJHYDENE.2008.11.014

Bodner, Hofer, A., & Hacker, V. (2015). H2 generation from alkaline electrolyzer. *Wiley Interdisciplinary Reviews. Energy and Environment*, *4*(4), 365–381. https://doi.org/10.1002/wene.150

Brunel. (2021). *The many colours of hydrogen energy: what they mean and which are best*. https://www.brunel.net/en-au/blog/renewable-energy/hydrogen-colours-explained

Carmo, M., Fritz, D. L., Mergel, J., & Stolten, D. (2013). A comprehensive review on PEM water electrolysis. *International Journal of Hydrogen Energy*, *38*(12), 4901–4934. https://doi.org/10.1016/J.IJHYDENE.2013.01.151

CoolProp. (n.d.). *Welcome to CoolProp*. http://www.coolprop.org/index.html

David, A., Mathiesen, B. V., Averfalk, H., Werner, S., & Lund, H. (2017). Heat Roadmap Europe: Large-Scale Electric Heat Pumps in District Heating Systems. *Energies 2017, Vol. 10, Page 578*, *10*(4), 578. https://doi.org/10.3390/EN10040578

Dong, Z. Y., Yang, J., Yu, L., Daiyan, R., & Amal, R. (2022). A green hydrogen credit framework for international green hydrogen trading towards a carbon neutral future. *International Journal of Hydrogen Energy*, *47*(2), 728–734. https://doi.org/10.1016/J.IJHYDENE.2021.10.084

EERE. (2017). *Hydrogen Production: Electrolysis*. Office of Energy Efficiency & Renewable Energy. https://www.energy.gov/eere/fuelcells/hydrogen-production-electrolysis%0Ahttps://energy.gov/eere/fuelcells/hydrogen-production-electrolysis

Ellevio. (2022). *Hur hög är energiskatten?* https://www.ellevio.se/privat/kundservice/faq/betalning/faktura-betalning/energiskatt/hur-hog-ar-energiskatten/

EIA. (2022). *Levelized Costs of New Generation Resources in the Annual Energy Outlook 2022*. U.S. Energy Information Administration. https://www.eia.gov/outlooks/aeo/pdf/electricity_generation.pdf

Eriksson, M., & Hallonsten, P. (2021). *Förslag till nationell strategi för fossilfri vätgas*. Energimyndigheten. https://www.energimyndigheten.se/nyhetsarkiv/2021/forslag-till-nationell-strategi-for-fossilfri-vatgas/

Falcão, D. S., & Pinto, A. M. F. R. (2020). A review on PEM electrolyzer modelling: Guidelines for beginners. *Journal of Cleaner Production*, *261*, 121184. https://doi.org/10.1016/J.JCLEPRO.2020.121184

Fragiacomo, P., & Genovese, M. (2019). Modeling and energy demand analysis of a scalable green hydrogen production system. *International Journal of Hydrogen Energy*, *44*(57), 30237–30255. https://doi.org/10.1016/J.IJHYDENE.2019.09.186

Fukuda, S., Kondou, C., Takata, N., & Koyama, S. (2014). Low GWP refrigerants R1234ze(E) and R1234ze(Z) for high temperature heat pumps. *International Journal of Refrigeration*, *40*, 161–173. https://doi.org/10.1016/J.IJREFRIG.2013.10.014

García-Valverde, R., Espinosa, N., & Urbina, A. (2012). Simple PEM water electrolyser model and experimental validation. *International Journal of Hydrogen Energy*, *37*(2), 1927–1938. https://doi.org/10.1016/J.IJHYDENE.2011.09.027

Geyer, R., Hangartner, D., Lindahl, M., & Vinther Pedersen, S. (2020). *Heat Pumps in District Heating and Cooling Systems - Final Report*. Heat Pump Centre. https://heatpumpingtechnologies.org/publications/heat-pumps-in-district-heating-and-cooling-systems-final-report/

Godula-Jopek, A. (2015). *Hydrogen Production: by Electrolysis*. John Wiley & Sons, Incorporated.

Government. (2021). *Sweden's climate policy framework*. Government Offices of Sweden. https://www.government.se/articles/2021/03/swedens-climate-policy-framework/

Granryd, E., Ekroth, I., Lundqvist, P., Melinder, Å., Palm, B., & Rohlin, P. (2009). *Refrigerating Engineering* (5th Edition). Royal Institute of Technology, KTH.

Hansen, K. (2019). Decision-making based on energy costs: Comparing levelized cost of energy and energy system costs. *Energy Strategy Reviews*, *24*, 68–82. https://doi.org/10.1016/J.ESR.2019.02.003

Hepbasli, A., Biyik, E., Ekren, O., Gunerhan, H., & Araz, M. (2014). A key review of wastewater source heat pump (WWSHP) systems. *Energy Conversion and Management*, *88*, 700–722. https://doi.org/10.1016/J.ENCONMAN.2014.08.065

HTP IEA. (n.d.). *Refrigerants*. Technology Collaboration Programme. https://heatpumpingtechnologies.org/market-technology/refrigerants/

Hu, B., Wu, D., Wang, L. W., & Wang, R. Z. (2017). Exergy analysis of R1234ze(Z) as high temperature heat pump working fluid with multi-stage compression. *Frontiers in Energy*, *11*(4), 493–502. https://doi.org/10.1007/S11708-017-0510-6

IEA. (2019). *The Future of Hydrogen: Seizing today´s opportunities*. OECD, Paris Cedex 16. https://doi.org/10.1787/1e0514c4-en

IEA. (2021). *Global Hydrogen Review 2021. IEA, Paris*. https://www.iea.org/reports/global-hydrogen-review-2021

Incropera, F. P., Dewitt, D. P., Bergman, T. L., & Lavine, A. S. (2013). *Principles of Heat and Mass Transfer* (7th Editio). John Wiley & Sons Singapore.

IRENA. (2020). *Climate Change*. https://irena.org/climatechange

Jouhara, H., Khordehgah, N., Almahmoud, S., Delpech, B., Chauhan, A., & Tassou, S. A. (2018). Waste heat recovery technologies and applications. *Thermal Science and Engineering Progress*, *6*, 268–289. https://doi.org/10.1016/J.TSEP.2018.04.017

Koroglu, E. O., Yoruklu, H. C., Demir, A., & Ozkaya, B. (2019). Scale-Up and Commercialization Issues of the MFCs: Challenges and Implications. *Biomass, Biofuels, Biochemicals: Microbial Electrochemical Technology: Sustainable Platform for Fuels, Chemicals and Remediation*, 565–583. https://doi.org/10.1016/B978-0-444-64052-9.00023-6

Lebbal, M. E., & Lecœuche, S. (2009). Identification and monitoring of a PEM electrolyser based on dynamical modelling. *International Journal of Hydrogen Energy*, *34*(14), 5992–5999. https://doi.org/10.1016/J.IJHYDENE.2009.02.003

Linde. (n.d.). *Köldmedia*. https://www.linde-gas.se/sv/products_ren/refrigerants/index.html

Lund, H., Werner, S., Wiltshire, R., Svendsen, S., Thorsen, J. E., Hvelplund, F., & Mathiesen, B. V. (2014). 4th Generation District Heating (4GDH): Integrating smart thermal grids into future sustainable energy systems. *Energy*, *68*, 1–11. https://doi.org/10.1016/J.ENERGY.2014.02.089

Makhnatch, P. (2014). *Low GWP refrigerants for high temperature heat pumps*. https://www.energy.kth.se/applied-thermodynamics/key-research-areas/heating-systems/low-gwp-news/koldmedier-med-lag-gwp-for-hogtemperaturvarmepumpar-1.501185

Marangio, F., Santarelli, M., & Calì, M. (2009). Theoretical model and experimental analysis of a high pressure PEM water electrolyser for hydrogen production. *International Journal of Hydrogen Energy*, *34*(3), 1143–1158. https://doi.org/10.1016/J.IJHYDENE.2008.11.083

Mathworks. (n.d.). *MATLAB*. https://www.mathworks.com/products/matlab.html

Moran, S. (2016). *Pump Sizing: Bridging the Gap Between Theory and Practice*. AIChE. https://www.aiche.org/resources/publications/cep/2016/december/pump-sizing-bridging-gap-between-theory-and-practice

Naimi, Y., & Antar, A. (2018). Hydrogen Generation by Water Electrolysis. *Advances In Hydrogen Generation Technologies*. https://doi.org/10.5772/INTECHOPEN.76814

Ninikas, K., Hytiris, N., Emmanuel, R., Aaen, B., & McMillan, S. (2014). A renewable heat solution for water ingress in the Glasgow subway tunnel system. *WIT Transactions on Ecology and the Environment*, *186*, 161–171. https://doi.org/10.2495/ESUS140141

Olivier, P., Bourasseau, C., & Bouamama, P. B. (2017). Low-temperature electrolysis system modelling: A review. *Renewable and Sustainable Energy Reviews*, *78*, 280–300. https://doi.org/10.1016/J.RSER.2017.03.099

Papapetrou, M., & Kosmadakis, G. (2022). Resource, environmental, and economic aspects of SGHE. *Salinity Gradient Heat Engines*, 319–353. https://doi.org/10.1016/B978-0-08-102847-6.00006-1

Pieper, H., Ommen, T., Buhler, F., Lava Paaske, B., Elmegaard, B., & Brix Markussen, W. (2018). Allocation of investment costs for large-scale heat pumps supplying district heating. *Energy Procedia*, *147*, 358–367. https://doi.org/10.1016/J.EGYPRO.2018.07.104

Ruuskanen, V., Koponen, J., Huoman, K., Kosonen, A., Niemelä, M., & Ahola, J. (2017). PEM water electrolyzer model for a power-hardware-in-loop simulator. *International Journal of Hydrogen Energy*, *42*(16), 10775–10784. https://doi.org/10.1016/J.IJHYDENE.2017.03.046

Sayegh, M. A., Jadwiszczak, P., Axcell, B. P., Niemierka, E., Bryś, K., & Jouhara, H. (2018). Heat pump placement, connection and operational modes in European district heating. *Energy and Buildings*, *166*, 122–144. https://doi.org/10.1016/J.ENBUILD.2018.02.006

Scheepers, F., Stähler, M., Stähler, A., Rauls, E., Müller, M., Carmo, M., & Lehnert, W. (2021). Temperature optimization for improving polymer electrolyte membrane-water electrolysis system efficiency. *Applied Energy*, *283*, 116270. https://doi.org/10.1016/J.APENERGY.2020.116270

SGH2. (n.d.). *Economics*. https://www.sgh2energy.com/economics

Shamoushaki, M., Niknam, P. H., Talluri, L., Manfrida, G., & Fiaschi, D. (2021). Development of Cost Correlations for the Economic Assessment of Power Plant Equipment. *Energies 2021, Vol. 14, Page 2665*, *14*(9), 2665. https://doi.org/10.3390/EN14092665

Shiva Kumar, S., & Himabindu, V. (2019). Hydrogen production by PEM water electrolysis – A review. *Materials Science for Energy Technologies*, *2*(3), 442–454. https://doi.org/10.1016/J.MSET.2019.03.002

Sohn, Y. J., Park, G. G., Yang, T. H., Yoon, Y. G., Lee, W. Y., Yim, S. D., & Kim, C. S. (2005). Operating characteristics of an air-cooling PEMFC for portable applications. *Journal of Power Sources*, *145*(2), 604–609. https://doi.org/10.1016/J.JPOWSOUR.2005.02.062

Sood, Prakash, O., Boukerdja, M., Dieulot, J.-Y., Ould-Bouamama, B., Bressel, M., & Gehin, A.-L. (2020). Generic Dynamical Model of PEM Electrolyser under Intermittent Sources. *Energies (Basel)*, *13*(24), 6556–. https://doi.org/10.3390/en13246556

Soupremanien, U., Le Person, S., Favre-Marinet, M., & Bultel, Y. (2012). Tools for designing the cooling system of a proton exchange membrane fuel cell. *Applied Thermal Engineering*, *40*, 161–173. https://doi.org/10.1016/J.APPLTHERMALENG.2012.02.008

SVI. (2021). *Stor potential för vätgasen i klimatomställningen*. Svensk verkstad. https://svenskverkstad.se/nyheter/Stor_potential_for_vatgasen_i_klimatomstallningen/65ke

Technologies. (n.d.). *Laminar Flow over a Flat Plate*. http://www.ttctech.com/Samples/Flatplate/flatplate.htm

Tiktak, W. J. (2019). *Heat Management of PEM Electrolysis*. Delft University of Technology. https://repository.tudelft.nl/islandora/object/uuid:c046820a-72bc-4f05-b72d-e60a3ecb8c89?collection=education

Ulleberg, Ø. (2003). Modeling of advanced alkaline electrolyzers: a system simulation approach. *International Journal of Hydrogen Energy*, *28*(1), 21–33. https://doi.org/10.1016/S0360-3199(02)00033-2

Wahlroos, M., Pärssinen, M., Manner, J., & Syri, S. (2017). Utilizing data center waste heat in district heating – Impacts on energy efficiency and prospects for low-temperature district heating networks. *Energy*, *140*, 1228–1238. https://doi.org/10.1016/J.ENERGY.2017.08.078

Werner, S. (2017). District heating and cooling in Sweden. *Energy*, *126*, 419–429. https://doi.org/10.1016/J.ENERGY.2017.03.052

Yigit, T., & Selamet, O. F. (2016). Mathematical modeling and dynamic Simulink simulation of high-pressure PEM electrolyzer system. *International Journal of Hydrogen Energy*, *41*(32), 13901–13914. https://doi.org/10.1016/J.IJHYDENE.2016.06.022

Zeng, K., & Zhang, D. (2010). Recent progress in alkaline water electrolysis for hydrogen production and applications. *Progress in Energy and Combustion Science*, *36*(3), 307–326. https://doi.org/10.1016/J.PECS.2009.11.002


Mälardalen
University